Bulletin of the Seismological Society of America, Vol. 100, No. 6, pp. –, December 2010, doi: 10.1785/0120090342

Neotectonics and Paleoseismology of the Limón and Pedro Miguel Faults in Panamá: Earthquake Hazard to the Panamá Canal

by Thomas Rockwell,[*] Eldon Gath, Tania González, Chris Madden, Danielle Verdugo, Caitlin Lippincott,[†] Tim Dawson,[‡] Lewis A. Owen, Markus Fuchs,[§] Ana Cadena, Pat Williams, Elise Weldon,[‖] and Pastora Franceschi

Abstract We present new geologic, tectonic geomorphic, and geochronologic data on the slip rate, timing, and size of past surface ruptures for the right-lateral Limón and Pedro Miguel faults in central Panamá. These faults are part of a system of conjugate faults that accommodate the internal deformation of Panamá resulting from the ongoing collision of Central and South America. There have been at least three surface ruptures on the Limón fault in the past 950–1400 years, with the most recent during the past 365 years. Displacement in this young event is at least 1.2 m (based on trenching) and may be 1.6–2 m (based on small channel offsets). A well-preserved 4.2 m offset suggests that the penultimate event also sustained significant displacement. The Holocene slip rate has averaged about 6 mm/yr, based on a 30-m offset terrace riser incised into a 5-ka abandoned channel.

The Pedro Miguel fault has sustained three surface ruptures in the past 1600 years, the most recent being the 2 May 1621 earthquake that partially destroyed Panamá Viejo. At least 2.1 m of slip occurred in this event near the Canal, with geomorphic offsets suggesting 2.5–3 m. The historic Camino de Cruces is offset 2.8 m, indicating multimeter displacement over at least 20 km of fault length. Channel offsets of 100–400 m, together with a climate-induced incision model, suggest a Late Quaternary slip rate of about 5 mm/yr, which is consistent with the paleoseismic results. Comparison of the timing of surface ruptures between the Limón and Pedro Miguel faults suggests that large earthquakes may rupture both faults with 2–3 m of displacement for over 40 km, such as are likely in earthquakes in the M 7 range. Altogether, our observations indicate that the Limón and Pedro Miguel faults represent a significant seismic hazard to central Panamá and, specifically, to the Canal and Panamá City.

Introduction

The geology of the Republic of Panamá in southeast Central America records the continuing collision between Central and South America (Fig. 1) (Mann and Corrigan, 1990; Silver *et al.*, 1990; Mann and Kolarsky, 1995; Coates *et al.*, 2004). The initial collision began in the Miocene, resulting in the development of the east Panamá deformed belt (Coates *et al.*, 2004) and continued with the oroclinal flexing of the isthmus and development of the north Panamá deformed belt in the Plio-Quaternary (Silver *et al.*, 1990; Mann and Kolarsky, 1995), along with the closing of the seaway between Central and South America in the Late Pliocene (Collins *et al.*, 1996). With a Global Positioning System (GPS)-measured rate between Central and South America of ~25 mm/yr (Trenkamp *et al.*, 2002), this ongoing deformation is distributed among faults throughout Panamá and western Colombia, resulting in internal deformation of the isthmus by folding and faulting. Many of the major faults of Panamá have long been recognized in the geology and geomorphology (Jones, 1950; Woodring, 1957; Stewart *et al.*, 1980), although they were not considered Holocene (Cowan, 1998, 1999; Schweig *et al.*, 1999; Petersen *et al.*, 2005). Among these, the Pedro Miguel, Limón, and related faults comprise a zone that extends from the southern flank of

*Also at the Department of Geological Sciences, San Diego State University, San Diego, California 92182.

[†]Now at CH2M-Hill, 25 New Chardon St. Suite 300, Boston, Massachusetts 02114.

[‡]Now at California Geological Survey, 345 Middlefield Rd., Menlo Park, California 94025.

[§]Now at the Geography Department, University of Bayreuth, D-95440 Bayreuth, Germany.

[‖]Now at the Department of Geological Sciences, University of Oregon, Eugene, Oregon 97403.

the Sierra Maestra in north-central Panamá southward for at least 40 km, crossing the Panamá Canal between the Miraflores and Pedro Miguel Locks, and extending southward offshore into the Gulf of Panamá (Fig. 1; Earth Consultants International, 2006).

The northern part of this zone comprises the Limón fault, which was first recognized by Jones (1950) (fault a-13 in his paper); and, although he only briefly discussed the fault, he did attribute the steepest gravity anomaly gradient across the Panamanian isthmus as being coincident with its location. Woodring (1957) mapped the Limón fault as a continuous (albeit sinuous) strand, whereas Stewart *et al.* (1980) mapped the Limón fault as two unnamed, discontinuous, right-stepping traces with a normal, down-to-the-east component. In the Cowan *et al.* (1998) map, the Limón fault is part of an unnamed fault system (fault number PA14) that is thought to be Quaternary in age, with an unknown rate of slip. It is noteworthy to mention that this map includes a fault offshore of the northern coast of Panamá, near the Panamá–Costa Rica border, that is also named the Limón fault. This offshore fault, which Cowan *et al.* (1998) indicate last ruptured in 1991, should not be confused with the Limón fault that is the subject of this study.

The Pedro Miguel fault was mapped as extending only about a kilometer south of the Panamá Canal (Woodring, 1957; Stewart *et al.*, 1980) with the Miocene La Boca formation faulted against Miocene basalt. Recent work by Earth Consultants International (2007) demonstrates that the fault continues much farther south, probably extending offshore into the Gulf of Panamá. North of the Panamá Canal, the fault is mapped to the north-northwest for about 12 km (Woodring, 1957; Stewart *et al.*, 1980), and Earth Consultants International (2006) has extended the fault to the Rio Chagres based on mapping of lineaments, geomorphology, and limited trenching.

As part of a seismic hazard characterization for the Panamá Canal Authority's (ACP) expansion project, we studied the geologic and geomorphic expression of the Pedro Miguel, Limón, and related faults, followed by an in-depth study into their Holocene earthquake and displacement history, critical factors in the design of the new locks and associated structures. In this paper, we discuss the geology and geomorphology of the Limón and Pedro Miguel faults separately, as they are distinct faults. For each, we present a general description of the geomorphology, followed by the paleoseismic results, including three-dimensional (3D) trenching to resolve slip. We also discuss our observations that relate to the Late Quaternary slip rate of these faults. We conclude with a discussion on the regional significance of these faults and their implications to the seismic hazard of central Panamá, including Panamá City and the Panamá Canal.

The Limón Fault

The Limón fault extends 20–25 km south from near its intersection with the Gatún fault to at least the Chagres River (Fig. 1 and Fig. 2). The northern connection of the Limón fault to the Gatún fault is obscured by the water levels at Lago Alajuela (also known as Madden Reservoir), complex geological relationships, and a lack of field exposures. The southern end of the Limón fault is also obscured because it lies directly within the Rio Chagres Valley. The fault is segmented into two distinct sections, as it makes a pronounced 3-km right bend at Nuevo Vigía, before continuing north to form the western shoreline of Lago Alajuela (Fig. 2).

We first identified and mapped the geomorphology along the Limón fault using a digital elevation model and aerial photography as part of a study to assess the likelihood

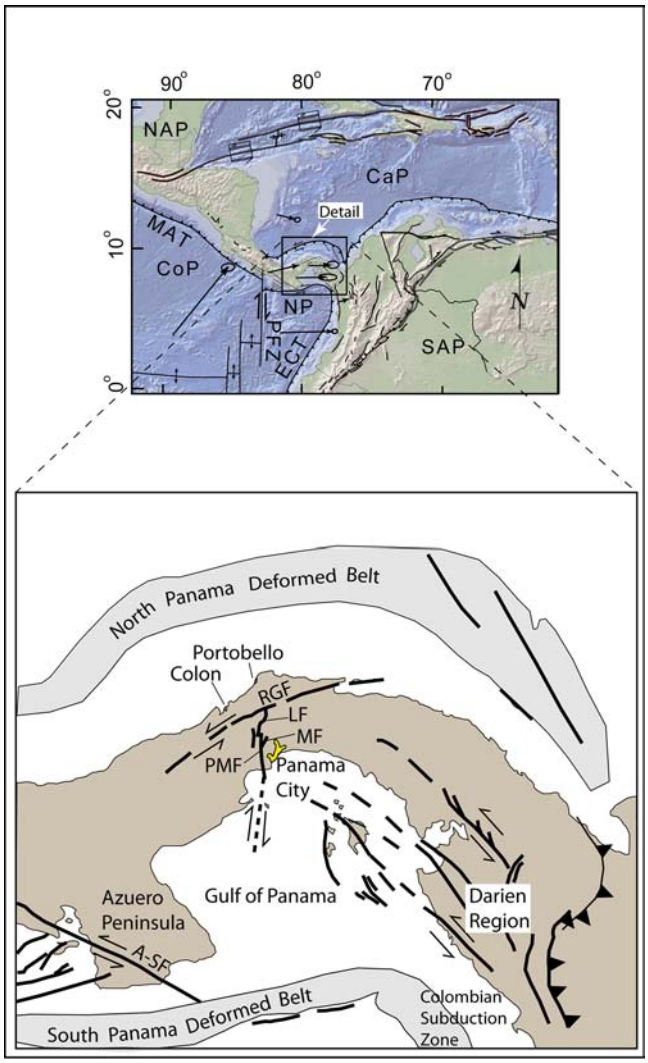

Figure 1. Location map of central Panamá, showing the Pedro Miguel (PMF), Limón (LF), Rio Gatún (RGF), Miraflores (MF), and Azuero-Sona (A-SF) faults. The inset provides the regional tectonic framework: NAP, North American plate; CaP, Caribbean plate; CoP, Cocos plate; PFZ, Panamá fracture zone; NP, Nazca plate; ECT, Ecuador–Colombian trench; SAP, South American plate. Arrows and circles represent the GPS velocities from the CASA campaign network relative to South America (see Trenkamp *et al.*, 2002). The color version of this figure is available only in the electronic edition.

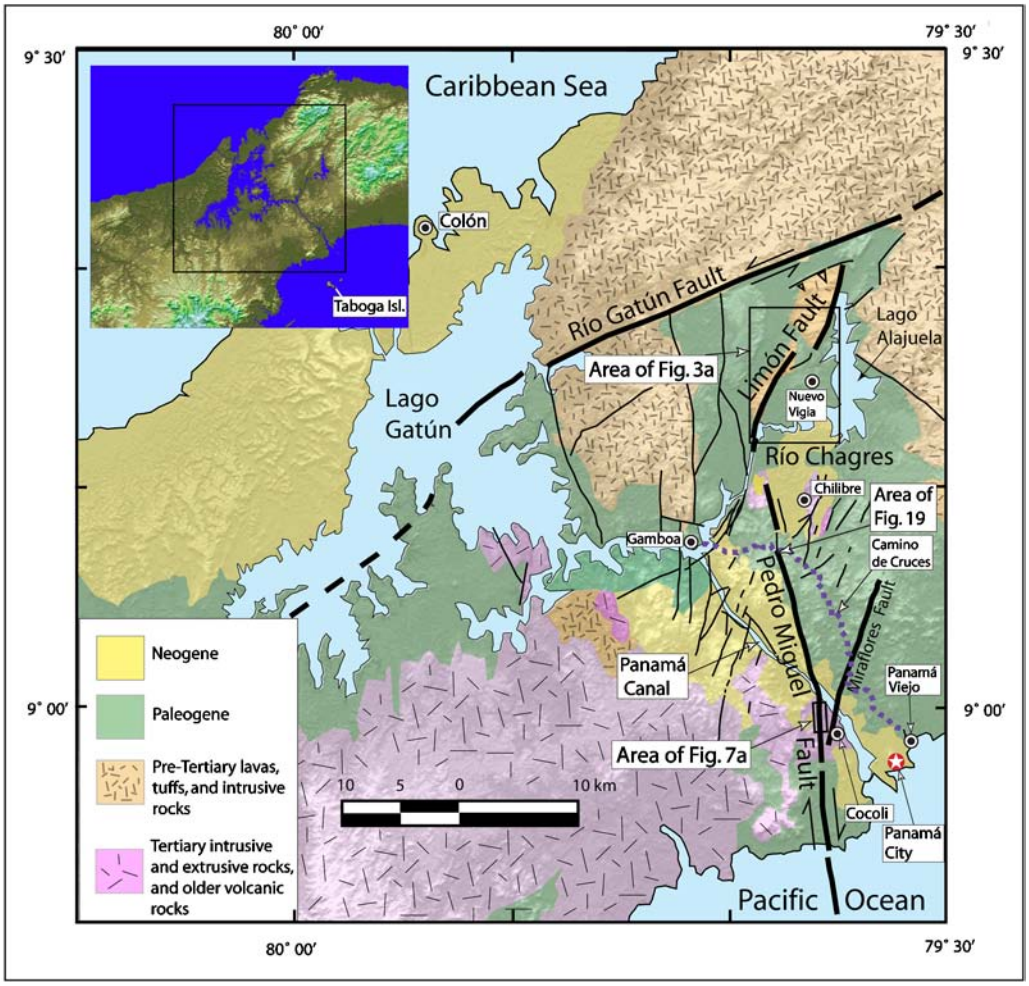

Figure 2. Map of central Panamá showing the geology and location of major faults superposed on a digital elevation model. The geologic units were grouped by age (Basement, Paleogene, Neogene) and are based on the mapping of Woodring (1957) and Stewert *et al.* (1980). The Limón and Pedro Miguel faults are shown, as are the Rio Gatún and Miraflores faults. Note that there are many small, unnamed faults also mapped in the vicinity of the Canal where exposures allowed for their recognition. The location of the branch of the Camino de Cruces that crosses the Pedro Miguel fault is indicated. The color version of this figure is available only in the electronic edition.

of the fault's activity and to search for potential trench sites (Fig. 2; Earth Consultants International, 2006, 2007). The Limón fault exhibits many of the classic landforms associated with active strike-slip faulting, including deflected and offset stream channels, beheaded channels, pressure ridges, aligned notches, linear valleys, and linear sidehill benches and troughs. Every stream that intersects the fault is right-laterally offset by varying distances, depending upon the age and size of the stream (Fig. 3), and many of the larger streams have a 1-m to 3-m-high knickpoint at or immediately upstream from the fault, reflecting either the difference in erodibility between the andesitic basalt and Tertiary sediments or a small normal component of slip on the fault. In addition to the offset streams, the ground surface shows evidence of small sidehill benches where the fault crosses the faces of slopes, a degraded moletrack from the last earthquake, displaced terrace risers, and small-scale extensional and compressional warping of the ground surface.

Paleoseismology and Slip Rate

We excavated two trenches across the geomorphic expression of the Limón fault north of the Río Chagres in an area of ranching and farming. Trench T1 was excavated across a linear depression where we expected to have a record of sedimentation. Trench T2 was excavated in a small drainage divide between two large deflected channels adjacent to the 1.6-m deflection of a small channel, so part of this exercise was to confirm the colocation of the fault and the deflected channel. A series of small hand-excavated fault-parallel trenches (trenchettes) were dug within the 1.6-m deflected channel to resolve displacement on the channel thalweg and to provide timing of the most recent surface rupture. The timing of past surface ruptures was determined largely from trench T1 and the small trenchettes in the deflection.

Trench T2 exposed the fault juxtaposing siltstone and claystone of the Caimito formation on the east against highly weathered and sheared andesitic basalt on the west (Fig. 4).

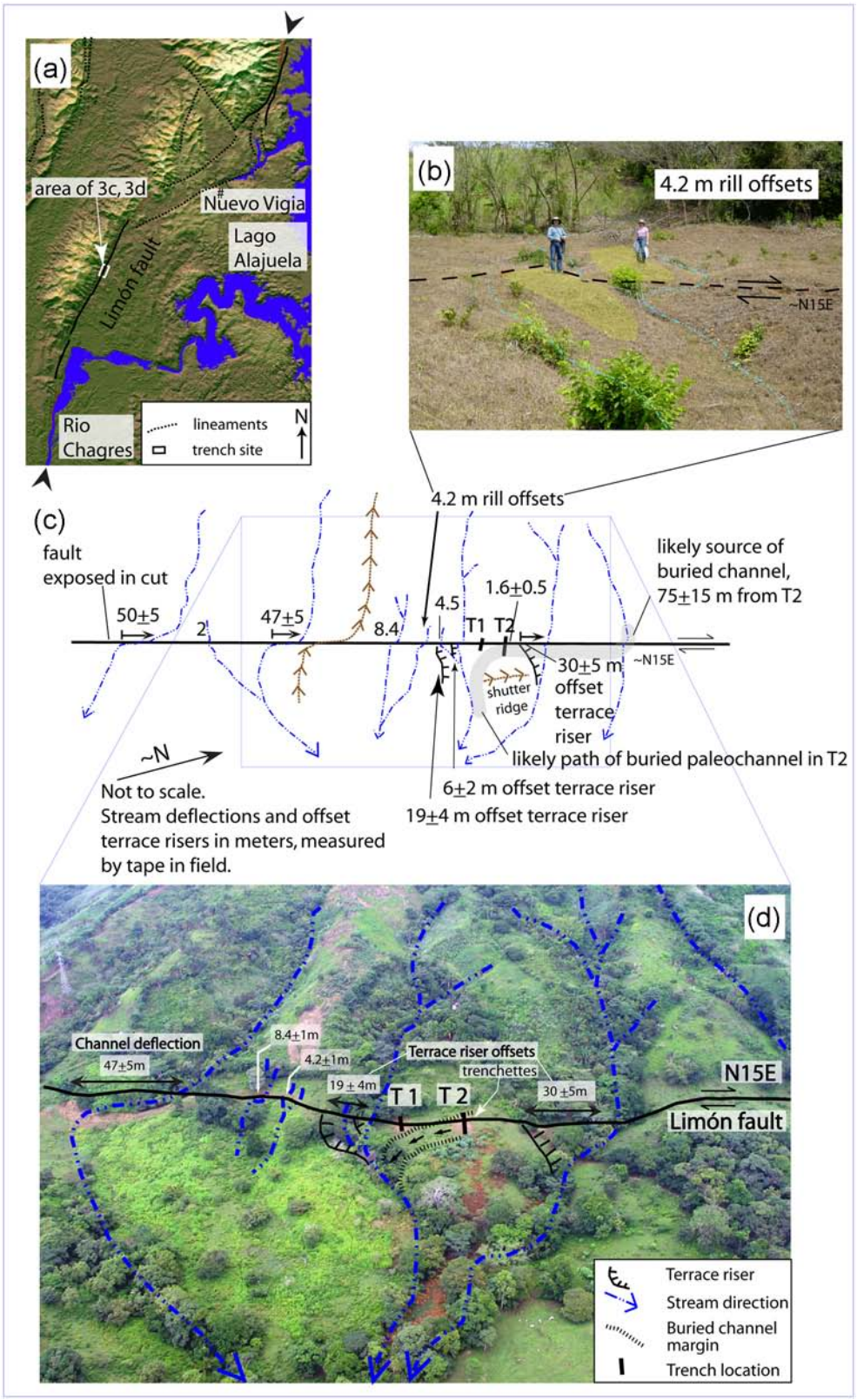

Figure 3. Detailed map of tectonic geomorphology near the trench site along the central Limón fault. (a) Detailed study area relative to the Chagres River and Lago Alajuela (Madden Reservoir). (b) A small rill offset, measured in the field as about 4.2 m of right-lateral offset. (c and d) Sketch of field-measured offsets and their correlation to an oblique aerial photograph. The arrows on streams in (c) indicate flow direction; the offset hatched line denotes a ridgeline. Note the locations of the trenches in (d). The color version of this figure is available only in the electronic edition.

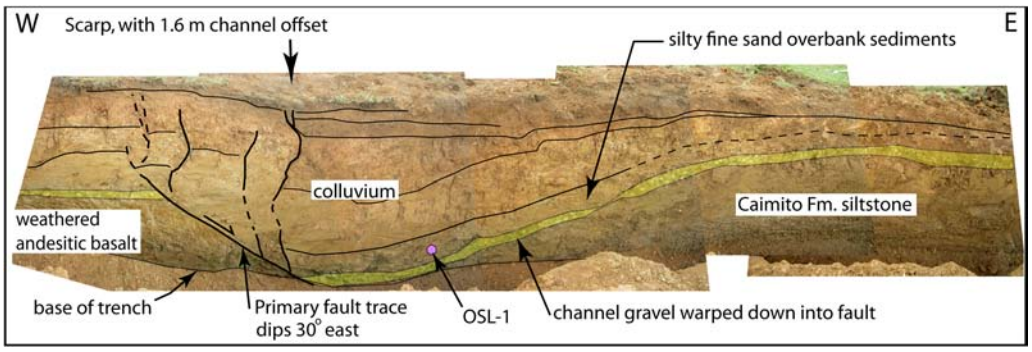

Figure 4. Log of the north face of trench T2 across the Limón fault at a small drainage divide (Fig. 3d). Note that the main fault juxtaposes Late Oligocene Caimito formation siltstone on the hanging wall against weathered andesitic basalt on the footwall. The primary fault was seen to dip at about 30° to the east, with a 2-m-wide zone of transtensive faulting near the fault tip. (W, west; E, east.) The color version of this figure is available only in the electronic edition.

The fault exhibits a low dip of about 30° in this exposure, and splays upward into a 2-m-wide zone of cracks in the upper 1–2 m from the surface. A distinctive cobble lag composed of 2–10-cm-sized andesitic basalt clasts is preserved on each side of the fault; this gravel is warped and faulted down into the fault zone. The cobbles are interpreted as the result of axial flow along the fault as they are preserved on both sides of the fault, and the channel margin was exposed in this trench about 2 m west of the fault zone. We argue that the gravels are sourced from a stream located about 75 m north of T2 (see Fig. 3), as that is the first drainage that we found to be transporting clasts of similar size and lithology. The cobble layer was capped by a silty fine sand deposit that is interpreted as the result of overbank sedimentation. We collected an optically stimulated luminescence (OSL) sample from this silty sand layer, which yielded an age of 5.0 ± 0.7 ka on quartz (Table 1). Considering that the cobbles are still hard and largely unweathered and that the rate of weathering in Panamá is rapid and severe (formation of oxisols under a tropical rainforest environment), we consider this as supporting evidence that the axial fluvial deposits are Holocene in age, corroborating the OSL dating. Furthermore, as discussed subsequently in this paper, paired radiocarbon and OSL ages from trench T1 yield similar dates (within a few hundred years), further substantiating the OSL age of the axial fluvial deposits.

Immediately north of the interfluve into which we excavated trench T2, there is a channel margin that slips off to the north in the direction of its source stream (Fig. 3). We interpret this channel margin as being laterally displaced by the Limón fault, with the terrace riser right-laterally offset 30 ± 5 m. Considering that the offset terrace riser is cut into the trenched interfluve, where the 5000-year-old stream gravel was exposed, the offset must have occurred after the stream capture that led to incision below this level. If the stream was actively flowing along the fault prior to capture, as seems reasonable, and if the terrace riser is close to the age of the incised terrace deposits, then this implies a slip rate of about $6\ ^{+2.1}_{-1.6}$ mm/yr, although this rate could also be interpreted as a minimum rate because the riser is younger than the actual age of the fluvial deposits preserved in the interfluve.

Table 1
Dates and Calibrated Ages for Radiocarbon and OSL Samples Collected from Limón Fault Exposures*

Sample Number	Laboratory Number	Stratigraphic Unit	^{14}C and OSL Ages (Years B.P.)	Calibrated Age (2σ)
Limón Trenchette	115887	surface channel	185 ± 35	A.D. 1640–1700 (20.8%) A.D. 1720–1820 (50.1%) A.D. 1830–1880 (5.8%) A.D. 1910–1960 (18.6%)
Limón T1-OSL-2		20b	1400 ± 200	
Limón T1 C-5	116288	50b	970 ± 40	A.D. 990–1160 (95.4%)
Limón T1 C-2	116036	50a	985 ± 35	A.D. 980–1160 (95.4%)
Limón T1 C-7	116037	60b	1430 ± 35	A.D. 560–660 (95.4%)
Limón T1-OSL-1		70	2000 ± 300	
Limón T1-OSL-3		85	1300 ± 200	
Limón T2-OSL-1		alluvium above bedrock in T2	5000 ± 700	

*Calendar ages are given for the 2σ (two sigma) intercepts for the ^{14}C dates; OSL sample ages are given as B.P.

Trench T1, excavated across a swale or depression at the base of the break in slope formed by the Limón fault, exposed multiple colluvial deposits in fault contact that we used to reconstruct the paleoearthquake chronology along this segment of the Limón fault (Fig. 5). Intensely sheared and weathered andesitic basalt bedrock (unit 500) was exposed west of the fault, whereas sheared and weathered clayey siltstone of the Caimito formation was exposed at the east end of the trench (unit 400; Fig. 5). These two bedrock units are expected to be in fault contact at shallow depth below the base of the trench exposure, as they were in trench T2. Near the ground surface, however, the fault is expressed as an approximately 6-m-wide zone of high-angle faulting that is bounded on the southeast by an antithetic fault. Numerous fault splays between the antithetic and main fault disrupt and displace colluvial units of varying ages. The structural relations between the main, south-dipping fault and the north-dipping antithetic fault have resulted in the formation of a graben along a negative flower structure that has been episodically filled with colluvium, preserving the paleoseismic record. We collected seven samples of detrital charcoal from these deposits, three of which were adequate for radiocarbon dating. We also collected three OSL samples to help constrain the ages of the faulting events and to compare with the radiocarbon results (Table 1).

The colluvial deposits have been repeatedly displaced by a number of faults that are interpreted as predominantly strike-slip, forming slivers of faulted colluvium and alluvium that have locally been faulted out of the plane of the exposure. Many of the units have clear mismatches in their thickness across individual fault strands, which is a clear indicator of strike-slip. As the deposits are primarily colluvial in nature,

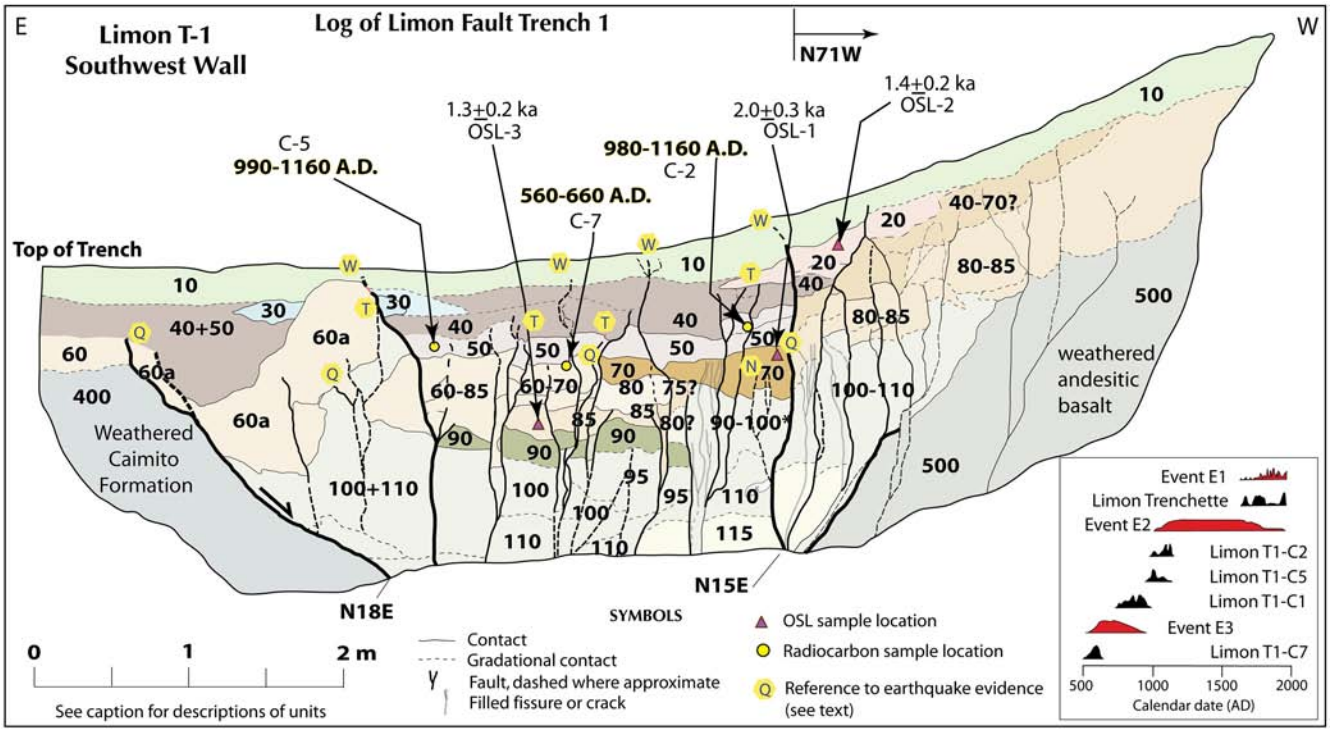

Figure 5. Log of trench T1 across the Limón fault, showing evidence for repeated Late Holocene displacements (Fig. 3d). See text for description and evidence of discrete events, which are indicated by letter (W, T, Q, N). Radiocarbon dates are in bold and calibrated to the AD time scale (OxCal v. 3.5, Ramsey, 2000), whereas the OSL dates are given in thousands of years before present (ka B.P.). The radiocarbon date and event pdfs are shown in the box at the lower right. Units are described as follows: 10—Modern topsoil (A horizon): silty fine to coarse sand with scattered pebbles; dark grayish brown; organic-rich; with abundant roots. 20—Colluvial wedge: silty sand to subangular pebble gravel; reddish brown. immediately postdates event T. 30—Colluvial wedge: associated with the penultimate event (event T); gray; source material and grain size vary from clayey silt to sand to coarse, angular pebble gravel. 40—Channel and graben fill: brown to grayish brown clay loam grading upward to organic-rich, dark grayish brown silty fine to coarse sand (A horizon); scattered pebbles. 50—Graben fill: clayey silt with pebble gravel and less than 1% volume of rounded cobbles; $CaCO_3$ present in matrix and coating clasts. 60—Channel deposit: yellowish brown fine sand with gravel; locally clast-supported; $CaCO_3$ coating some clasts; capped by an A soil horizon. 70—Colluvial wedge: light brownish gray clayey silt to sandy clay with coarse sand and pebbles; $CaCO_3$ coating clasts; capped by an A soil horizon. 80—Colluvium: light yellowish brown clayey silt to silty clay with sand and pebble gravel; $CaCO_3$ present in matrix and coating clasts. 90—Buried organic soil: grayish brown clay to sandy clay with scattered gravel. 95—Colluvial graben fill: grayish brown clayey silt, fine sand, and coarse pebble gravel. 100,110—Undifferentiated colluvium: light grayish brown, massive clayey silt and sand to fine pebble gravel; contains dark manganese oxide nodules. 115—Colluvium: light gray clayey silt to sand with rounded pebble gravel; $CaCO_3$ coating clasts. 400—Caimito formation: clayey siltstone; gray to olive gray; highly weathered and sheared. 500—andesitic basalt (bedrock): weathered and highly sheared; locally reduced to a fine sandstone in appearance. The color version of this figure is available only in the electronic edition.

the fine resolution of stratigraphy and exact placement of event horizons was difficult to resolve. Nevertheless, we used color and textural differences to identify as many as 15 different colluvial and alluvial deposits in the graben (units 10—115). Some of these colluvial sediments (i.e., units 20 and 50; see Fig. 5) consist of reworked, weathered clasts of andesitic basalt, whereas others appear to consist of reworked weathered siltstone and claystone of the Caimito formation mixed in with the basalt clasts. We also used the presence of buried soils (as are present capping units 40, 60/70, and 90) to distinguish former surfaces. In the following paragraphs, we describe the evidence for each recognized surface rupture, from the ground surface to the bottom of the trench, with the caveat that we may have missed evidence for some slip events due to the generally massive and bioturbated nature of the colluvial sediments.

The most recent event, herein named event W, ruptures nearly to the surface on several fault strands. In fact, it probably did rupture all the way to the surface through unit 10, based on the presence of a surface scarp and micromorphology associated with a degraded moletrack (rupture trace), but active mixing processes in the surface soil, along with continued colluvial deposition, likely have obscured the fault trace in the upper 10–20 cm. Several fault strands that ruptured in event W clearly displace the base of unit 10 and all lower units.

Charcoal was not present in units 10 or 20 to place constraints on the youthfulness of event W in trench T1. However, the trenchettes across the small, displaced channel about 3 m north-northeast of trench T2 (Fig. 3) contained abundant charcoal that we use to constrain the timing of the most recent event (Fig. 6). Samples of detrital charcoal were collected from this displaced channel for radiometric analysis, which placed the age of this event as post-AD 1640 (Table 1). However, the density of charcoal suggests that it originated from burning and clear-cutting of the forest during establishment of the local ranch during the nineteenth century. Thus, event W is historical in age, and slip on this fault should be associated with one of the historically reported events, such as a poorly known earthquake in 1849 that collapsed stone buildings in Panamá City, an 1855 event that reportedly was felt in Colón, Gatún, and Panamá City, or the 1873 event that was also felt both in Panamá City and Colón, and strongly shook the bridge over the Río Chagres. A possible fourth alternative is rupture during an aftershock of the great (*M* 7.9) 1882 earthquake.

To resolve slip for event W, we hand-excavated five small trenches (trenchettes) in the area of the offset channel, with their axes perpendicular to the channel and parallel to the fault. Two of these trenchettes were most helpful for this study, exposing the edge of the charcoal-bearing channel deposit that is offset by the Limón fault, as discussed in the preceding paragraphs. Using the southwestern edge of the channel as a piercing point, we measured a minimum of 1.2 meters of brittle right-lateral slip for event W on this fault (Fig. 6). Because the trenchettes were excavated to within

Figure 6. Interpreted photographs of the small, 1.6–2 m offset swale, located a few meters north of trench T2. Several small trenchettes (Fig. 3d) exposed a charcoal-bearing buried channel from which we resolved a minimum of 1.2 m of brittle slip on one of the fault strands. The swale is deflected 1.6 m, with a maximum of about 2 m. The color version of this figure is available only in the electronic edition.

centimeters of the primary fault trace, the uncertainty for this displacement is small. Observations of this swale prior to trenching suggested the presence of two main fault traces: a western one offsetting the swale approximately 1.6 meters

and an eastern trace offsetting the swale an additional 0.4 m, for a total displacement of about 2 m. The western strand with 1.6 m of apparent deflection corresponds to the minimum of 1.2 m of brittle displacement resolved in the trenchettes. For the eastern strand, the other trenchettes were less definitive, as we did not observe distinct channel deposits with clear edges that we could use as piercing points. Therefore, from this exercise, we determined that the minimum lateral displacement for event W on the Limón fault at this location is 1.2 m, although as much as 1.6–2 m are likely from the geomorphology (this would include near-field plastic deformations).

The penultimate event recognized in trench T1, designated herein as event T, produced rupture on several fault strands near the northern side of the graben that displace units 40 and below and are overlain by unit 20. There are other fault strands within the graben that displace the base of unit 40 but could not be traced upward very far and which do not offset the base of unit 10. Further, a colluvial wedge (unit 30) was apparently generated by production off a scarp from this event on one of the main faults bounding the graben on the south. A T symbol within an octagon is used in Figure 5 to show where evidence for event T is fairly clear. In all, as many as five fault strands may have ruptured in event T.

The age for event T is poorly constrained by two radiocarbon dates from unit 50. These ages are consistent and nearly identical (Table 1) at about AD 1060 (AD 980–1160 at 2σ, based on our OxCal model shown in Fig. 5), and they indicate that event T occurred between AD 1060 and the age of the channel offset in the trenchettes, dated as post-AD 1640. We also submitted OSL samples from units 20 and 70 that should have helped constrain the timing of this event. However, both samples yielded an age that is several hundred years older than the radiocarbon results. We interpret these OSL results to reflect the role of inheritance that is common in rapidly deposited colluvial deposits that have not been completely bleached prior to deposition. Additionally, the dose rates obtained from the deposits were low, probably reflecting severe leaching of the natural radiogenic minerals because of the high tropical precipitation, and therefore the OSL results should be viewed as maximum ages due to this potential problem. Nevertheless, the fact that the OSL and radiocarbon results are similar indicates that inheritance is small. This is an important observation when considering the ~5 ka age of the fluvial deposits in T2 and its implications for the slip rate.

The third oldest event interpreted from this trench exposure is designated as event Q and is so indicated on Figure 5. This event apparently occurred when the top of unit 70 was at the surface on the west side of the graben and unit 60 was at the surface on the east side. Units 60 and 70 darken to the surface, which we infer as evidence that an A soil horizon caps these units, indicating the occurrence of some time between deposition of these units and the overlying unit 50. Furthermore, this appears to have been a large event that produced a significant scarp that generated the deposition of units 40 and 50. Unit 40 is interpreted as the A horizon developed in colluvial unit 50, based on darkening of the soil material upward to the top of unit 40. On the west side of the graben, unit 50 fills against and is bounded by the fault, whereas unit 40 is present across the fault (and was subsequently offset in events T and W).

Several fault strands and fissures, denoted with a Q in Figure 5, apparently ruptured within the graben itself. Some of these display significant mismatches in stratigraphic thickness across them, indicative of significant lateral slip. On the east side of the graben, unit 60a was apparently backrotated along the antithetic fault by a substantial amount, after which clay-rich unit 40 + 50 accumulated in the depression produced by this backrotation. The fault is dashed, as we could not discern whether this was the actual slip surface or a degraded scarp. The observation that the main antithetic fault has not reruptured since event Q also argues that this may have been a larger event than either of the subsequent ruptures.

The timing of event Q is constrained by a radiocarbon age from unit 60 as postdating AD 560 (2σ range AD 560–660) but predating the two radiocarbon ages from unit 50 (AD 980–1160; Fig. 5). An OSL age from unit 85 (1.3 ± 0.2 ka) (Table 1) is consistent with these radiocarbon ages but suggests that the event falls toward the younger end of the possible age range. Thus, event Q occurred between AD 560 and 1160 but was more likely after about AD 700, based on the OSL age of unit 85 (which provides a maximum age).

Evidence for older events is also present in trench T1, but the ages of the alluvial and colluvial units are currently unconstrained. One event designated as event N drops the base of unit 70 (a buried topsoil) along the western graben-bounding fault and resulted in deposition of more soil to produce the wedge-shaped colluvial deposit of unit 70. Other fault strands are seen to offset the base of unit 70 but not the top. These observations indicate that the event occurred within unit 70 itself.

Below unit 70, we are less confident on the rupture history, given that weathering and repeated rupture by subsequent earthquakes has obscured unit correlations. One possible event is suggested by fault strands that offset and drop unit 80 but do not break unit 70 within the graben, about 0.5 m east of the main western graben-bounding fault. Another older event is inferred to break units below unit 90, which is interpreted as another buried topsoil. Unit 90 itself may have been down-faulted at the graben margin, but that relationship is now obscured by subsequent events. Finally, there are stratigraphic units, such as units 90 and 95, which appear to be accumulations within the graben that could be sedimentation after an event. However, as lateral slip is the dominant sense of motion, we are not confident as to the origin and extent of these units.

In summary, three surface ruptures have occurred on the Limón fault in the past ~950 to 1400 years, two in the past ~370 to 950 years, and one in the past 370 years. The most recent event W was associated with a minimum of 1.2 m of right-lateral slip and may have had as much as 2 m of displacement. A nearby channel is deflected about 4.2 m

(Fig. 3), suggesting a potentially larger amount of displacement in the penultimate event. Although poorly dated at present, the results do show recurrent Late Holocene rupture. Calculations using the 95% confidence ranges on the interval ages of the timing of the earthquakes yields an average recurrence interval of 450–600 years, based on only three events.

The Pedro Miguel Fault

The Pedro Miguel fault has been previously mapped as a structural boundary (Fig. 2) (Woodring, 1957; Stewart *et al.*, 1980) south and west of the Panamá Canal as the contact between the post-early Miocene basalt and the Early Miocene La Boca formation. North of the Canal, it is mapped as forming the contact between the Early Miocene Las Cascadas and the Early Oligocene Panamá formations, while farther north, it lies entirely within the Late Oligocene Caraba formation, with a possible northern extension cutting the La Boca and Las Cascadas formations.

Our geomorphic analysis suggests that the Pedro Miguel fault is longer than originally mapped by Woodring (1957). We found that the fault likely continues southward offshore into the Pacific Ocean where Taboga Island (see inset in Fig. 2) may indicate an uplift at a left step on the fault. To the north, the fault extends at least to the vicinity of the town of Chilibre, making the onshore length of the fault at least 30 km. North of Chilibre, the fault expression becomes weak, suggesting that it dies out, steps slip west to the southern extension of the Limón fault, or steps slip east to a horsetail splay of faults south of Lake Alajuela.

The geomorphic expression of the Pedro Miguel fault is good to fair, with this subdued signature in part due to an absence of a vertical component of slip on the fault and also to the general absence of a resistant rock (such as basalt) on only one side of the fault along most of its length. Nevertheless, the fault is expressed geomorphically by an alignment of linear valleys, ridges, and escarpments and is generally visible through the rainforest cover. Several offset and deflected drainages show that the fault experiences principally right-lateral motion, and this sense of motion is clear in the Cocolí area immediately south of the Panamá Canal.

Slip Rate of the Pedro Miguel Fault

At Cocolí, the most recent channel incisions in two parallel, east-flowing Late Quaternary drainages are both right-laterally offset 100 ± 20 meters by the north-striking Pedro Miguel fault (Fig. 7). This estimate of displacement is based on reconstructions using the 1914 topographic maps of the area that show the channel morphology prior to any significant earth moving in the 1940s associated with the Third Locks project (Fig. 7).

The northern drainage exhibits more deflection, about 200 m, than the southern channel if a low terrace to the northern drainage is considered (Fig. 7). However, the southern drainage is underfit for its drainage area and likely is offset from the northern drainage source, a distance of about 400 m. If correct, then there should be fluvial deposits flowing along the fault that are preserved in the interfluve region between the two channels. To test this, we excavated a number of trenches in the interfluve area to map out the fault zone and find the fluvial gravels, if present. Figure 8 shows the location of the fault zone through the interfluve area between the two deflected channels, as exposed in several trenches, and there are indeed fluvial gravels preserved (Fig. 9) that reflect flow from the northern channel drainage area to the underfit southern channel mouth. With the addition of three fault-parallel trenches, we distinguished three separate channelized fluvial deposits, Qoal1, Qoal2, and Qoal3 (Fig. 8) that are all interpreted to have originated from source channel B in Figure 7.

The fault zone bounds the fluvial deposits on the west, indicating that these channels are truncated by the fault and displaced laterally from their source. Qoal2 and Qoal3 are bound by the primary fault, whereas Qoal1 is bound on the west by a high-angle secondary strand, and this channel unit is found only within the fault zone (Fig. 8). The Qoal3 deposit is composed of subangular clasts of basalt in a mottled gray and red clayey matrix, channels Qoal1 and Qoal2 contained a basal gravel composed of subrounded clasts capped by highly weathered reddened finer deposits. The channels represent flow along and east of the fault prior to the capture of the current drainage system. Thus, there has been as much as 200 m of postcapture displacement on these channels, with as much as 100 m of post-deep incision displacement on both modern channels.

We attempted to date the three channel deposits with OSL because we recovered no detrital charcoal from any of the channel deposits. However, the quartz used in the OSL dating produced an unstable signal, which calls into question the validity of these OSL ages, so we did not use them for calculation of a slip rate.

To provide some constraints on the ages of the offset channels and to place a first-order constraint on the longer-term slip rate of the fault, we invoke a climate-driven stream incision model. The deflected channels at Cocolí grade to the primary drainage, the Río Cocolí, which in turn is graded to sea level. This site is only a few kilometers from the coast, so a major drop in sea level would be expected to induce significant incision of the Río Cocolí and its primary tributaries because a lowered base level results in higher stream gradients, which increase stream power. Considering that sea level was at or near its minima for the period between about 23 and 15 ka (Bard *et al.*, 1996), we infer that the modern channels (A-A' and B-B') correspond to incision and erosion during this last major eustatic sea level lowstand. We also infer that this is when the southern channel (channel A-A' in Fig. 7) had sufficient stream power to initiate significant headward erosion into the basalt west of the fault. Backfilling of the channels during sea level rise at the close of the Pleistocene has

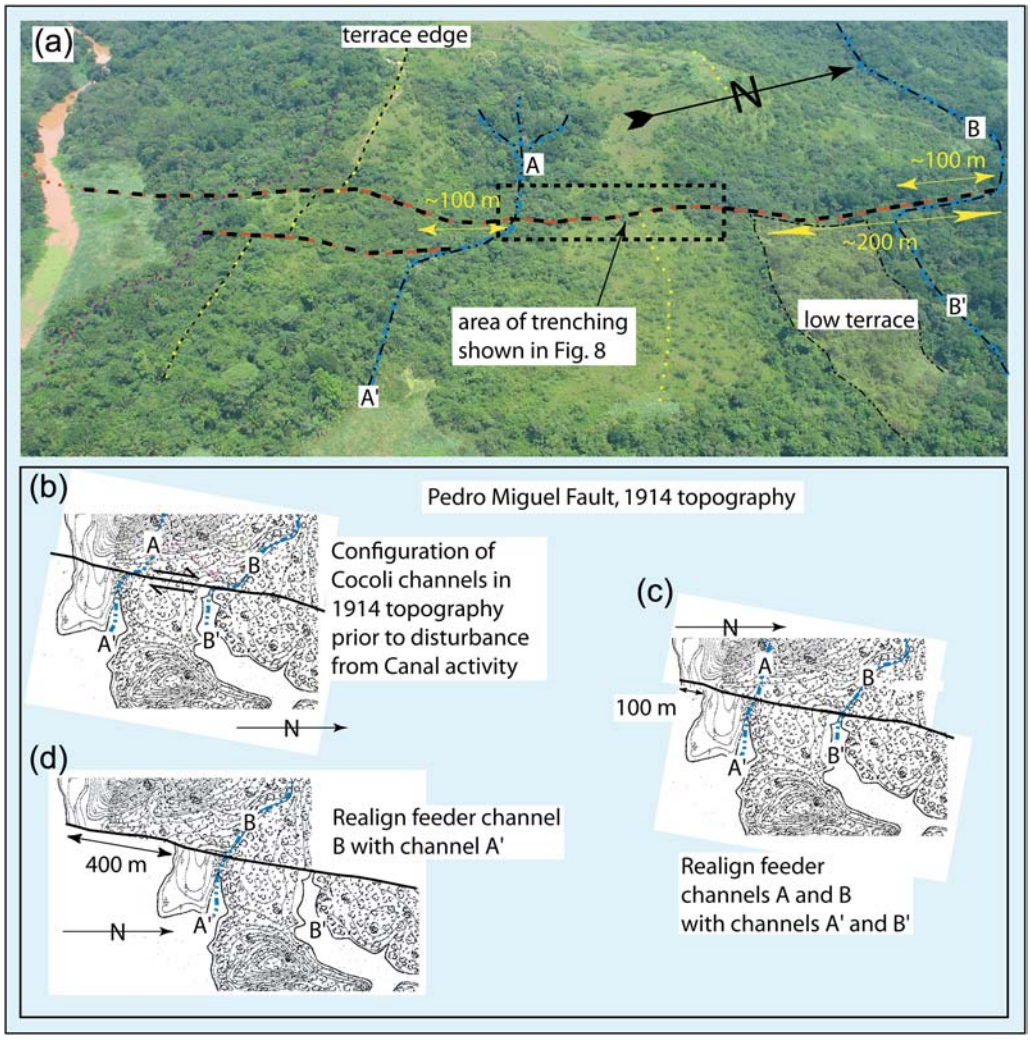

Figure 7. (a) Interpreted oblique aerial photograph of the Pedro Miguel fault in the Cocolí area south of the Panamá Canal, with the area of detailed trenching shown in Figure 8 indicated by the dashed black box. (b) The 1914 topographic map of these offsets, with their reconstruction shown in (c) by 100 m and in (d) by 400 m. The color version of this figure is available only in the electronic edition.

resulted in broad, alluvial-filled channel mouths; this is particularly apparent for the southern, underfit channel (Fig. 7).

Postincision motion on the Pedro Miguel fault has resulted in the current configuration with about 100 ± 20 m of offset of both channels A and B. If we are correct that the incision event corresponds to the last major eustatic sea level low stand at 19 ± 4 ka, this yields a Late Quaternary slip rate of 3.5–8.0 mm/yr.

The age of the initial incision may be as much as twice as old if the incision is the result of stream capture. Stream captures are more likely during periods of relatively high sea level, as the channels are presumably graded to the higher base level and have the greater potential to spill across to a steeper drainage that may be juxtaposed to the offset drainage source. With this model, the initial capture may have occurred during the stage 3 high-stand at ~45 ka. If the low terrace in the northern drainage corresponds to this event, and we use the 200 ± 30 m of deflection on the terrace edge as postcapture displacement, this suggests a similar ~5 mm/yr rate.

Paleoseismology

We excavated several sites where sufficient stratigraphy was present to either resolve the timing of the past several events or to resolve displacement through 3D trenching, so as to place constraints on the plausible size of future earthquakes. The main active trace of the Pedro Miguel fault strikes an average of N12°W, from the Río Chagres to the southern margin of Miraflores Lake (Fig. 2). South of the lake near Cocolí, the main fault strand is expressed as an en echelon series of transpressive petals exploiting the west-dipping bedding planes of the La Boca formation. This main strand is approximately coincident with, though easterly of, the contact between the Early Miocene La Boca formation to the east and slightly younger basalt to the west. At greater depth, the fault likely forms the La Boca formation/basalt contact.

We concentrated on the main trace, which was strongly expressed in the landscape morphology, as described previously. Several small, 2–3-m right-lateral stream deflections (subsequently confirmed by trenching) were present along

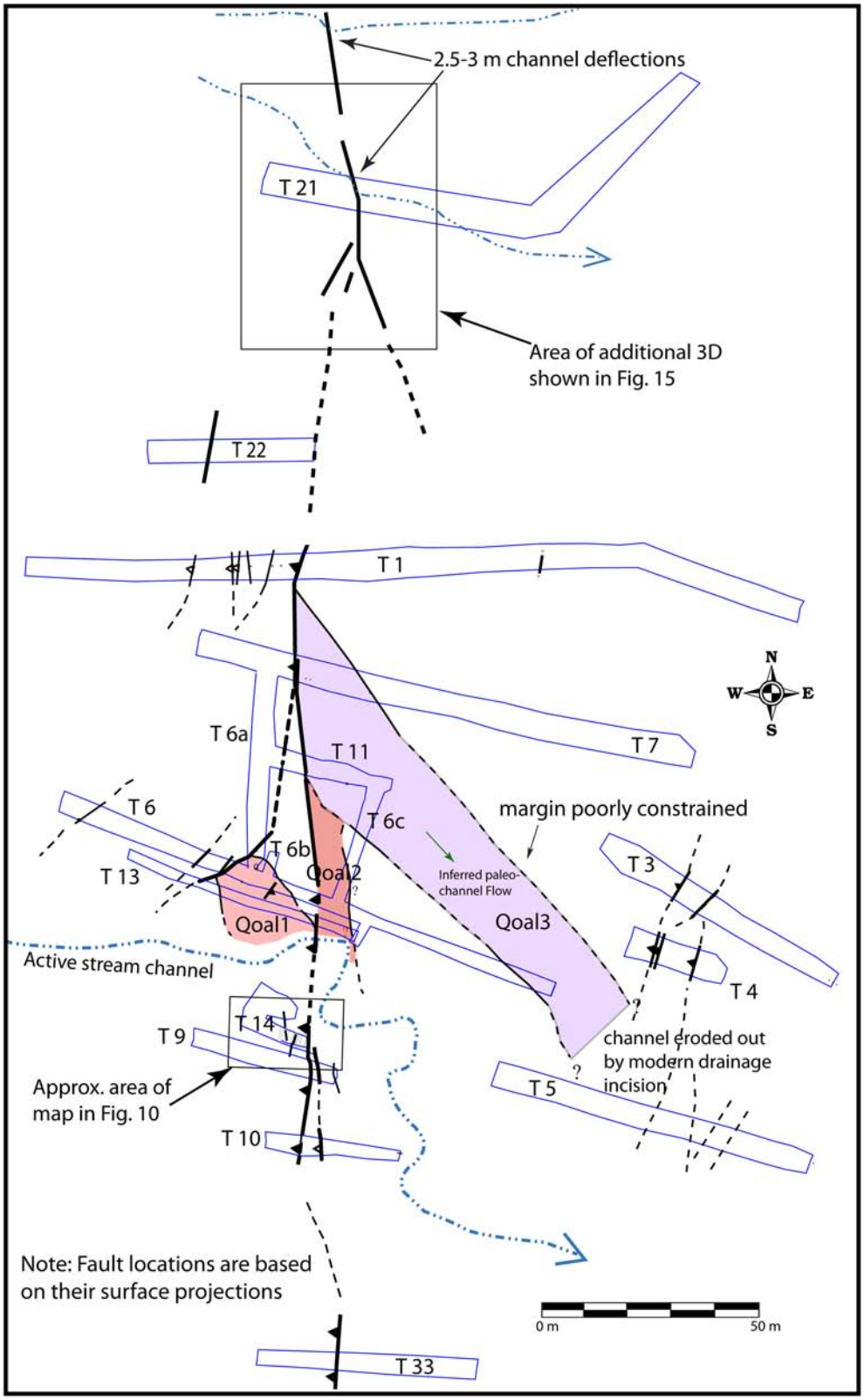

Figure 8. Map of trenches that we used to map the fault and displaced channels in the interfluve area between channels A and B (Fig. 7) in the Cocolí area. Note also the locations of T14 and T21, where we conducted detailed 3D excavations to resolve displacement per event. The color version of this figure is available only in the electronic edition.

the main Pedro Miguel fault in the Cocolí area. One of these was developed into a 3D trench site (trench T21; see Fig. 8) to confirm that the deflection reflected actual displacement. Another 3D site at trench T14 (see Fig. 8) was developed adjacent to a larger channel deflection. The Pedro Miguel fault zone is locally broad through the Cocolí area where we conducted all of the 3D work. The primary fault at both locations is low-angle, dipping about 30° to the west with multiple strands stepping from one bedding surface to another within the La Boca formation. Thus, the displacements determined from 3D trenching in this area probably reflect minimum values. Nevertheless, they provide solid information on the sense of slip, as well as timing, for past events. In the following section, we discuss each of the two 3D sites separately and then combine the interpretations into a common rupture history.

Timing and Displacement of Buried Channels at the T14 Site

Trenches T9 and T14 were excavated south of the main interfluve area discussed previously, immediately south of drainage A-A' in Figure 7, with T14 located only a couple of meters north of T9 (Fig. 8 and Fig. 10). Both trenches exposed the primary trace of the Pedro Miguel fault, which in this area dips shallowly to the west, and several high-angle faults that are transfer structures between the stepping low-angle primary faults.

Trench T9 exposed a sequence of nested gravelly channel and colluvial deposits located a few meters east (downslope) from the fault (Fig. 11a). Trench T14 (Fig. 11b) exposed the same gravel and colluvial units with much better stratigraphic resolution. Most of these units in T14 were obliquely overthrust by the La Boca formation bedrock, and structural and stratigraphic relations suggested evidence of recurrent motion with up to three preserved events, as is discussed subsequently in this paper. Also of interest was the observation that the edge of the upper channel deposit (unit 6) was closer to the fault in trench T14 than observed in trench T9, suggesting that if this trend continued northward, the channel could intersect the fault and provide a potential piercing point to resolve slip. To investigate this, we excavated two additional trenches to the north, labeled T14a and T14b (Fig. 10 and Fig. 11c,d). As each successive cut to the north is closer to the active drainage, the stratigraphic section is expected to young to the north, a consideration that must be kept in mind in the ensuing discussion.

We divided the stratigraphy into ten primary units and several secondary units based mainly on the presence or absence of grain-supported gravel deposits, contrasts in color, obvious changes in texture, and the presence of buried topsoil/colluvial units that are interpreted to represent past ground surfaces. Unit 1 is the modern topsoil (A horizon) and is interpreted to be partly colluvial in nature. Unit 2 is a gravelly channel that was present above the fault in trenches T14 and T14a, with its base in fault contact, indicating that unit 2 predates the most recent surface rupture. In trench T9, this deposit was situated only on the footwall (east) side of the fault. These relationships indicate right-lateral strike-slip; however, because the edges of the unit 2 channel had been removed during excavation of trenches T9 and T14, we did not try to use this as a piercing point due to the large uncertainties.

Units 3 through 5 represent a sequence of colluvial soils and minor fine-gravel channel alluvium that, in part, fill or cap the channel deposits of unit 6. Unit 6 is subdivided into

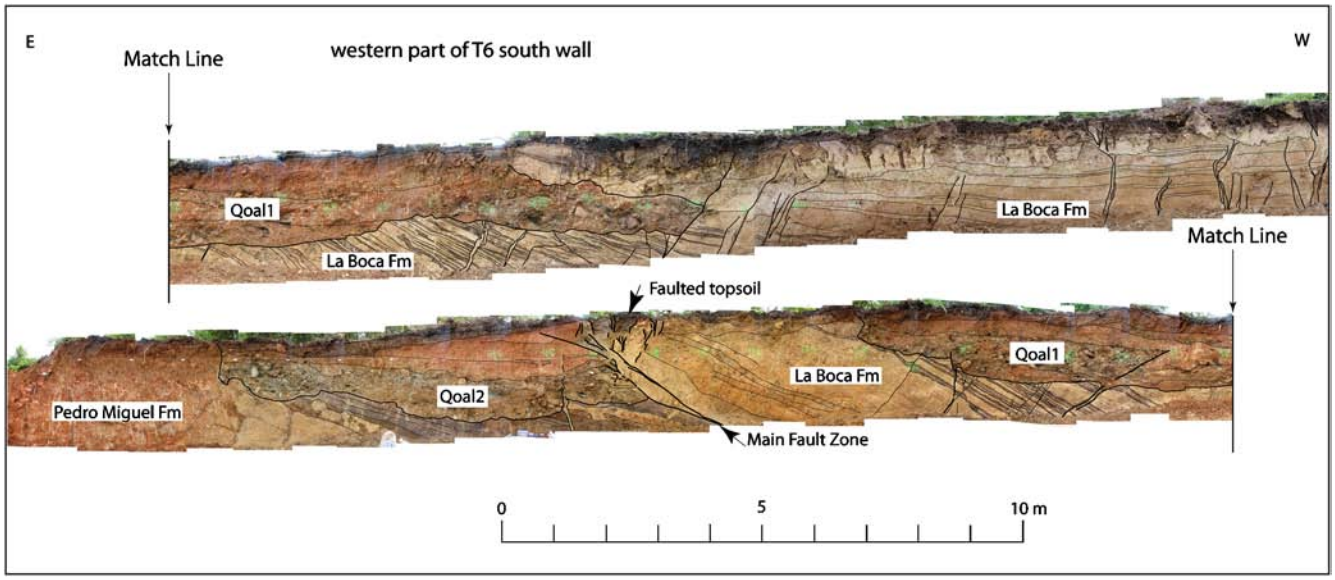

Figure 9. Interpreted photomosaic of a portion of trench T6 (see Fig. 8 for location), showing channels Qoal1 and Qoal2. Note that in addition to the main fault zone, numerous secondary faults break the La Boca formation, with some also displacing the paleochannel deposits. The color version of this figure is available only in the electronic edition.

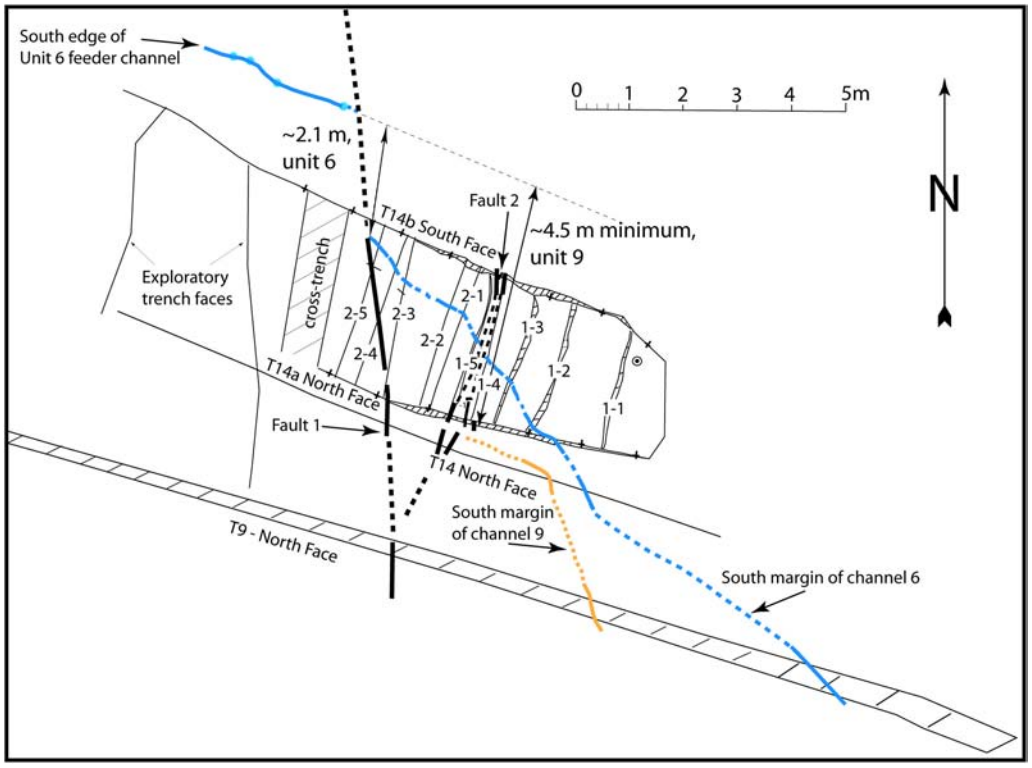

Figure 10. The T14 3D trenches (see Fig. 8). The southern margin of unit 6 gravel is indicated on both sides of the fault, whereas the southern margin of the unit 9 gravel is truncated at the eastern fault strand. The locations of the individual slices shown in Figure 13 are indicated. Slip on the unit 6 channel is measured in the slip direction, as the fault expresses oblique slip at this site. Slip for the unit 9 channel is a minimum, as the location of the feeder channel is unknown but must be no farther south than the unit 6 feeder channel west of the fault. The color version of this figure is available only in the electronic edition.

two subunits, 6a and 6b, with 6b representing the basal gravel and 6a representing the channel fill. Unit 6 is one of the two channels for which displacement was resolved. Units 7 and 8 are fine-grained, organic-enriched clayey silt deposits that are interpreted as colluvial and soil units, respectively, that accumulated during a period between gravel deposition. Unit 9 is the lower major gravel interpreted as the axial channel deposit for the primary drainage and is the older of the two channels for which we resolved displacement. Unit 10 is a buried topsoil unit developed into the underlying bedrock. This is important because one of the interpreted paleoearthquakes postdates unit 10 at the fault, as discussed in the Event 3 section. In the following discussion, we refer primarily to the channel deposits of units 6 and 9.

Age of Alluvium in the Trench T14 Site

The many trenches at the T9 and T14 site exposed numerous pieces of detrital charcoal, with charcoal occurring in nearly every unit. For carbon dating, we initially selected a suite of 12 samples from trench T14, using samples from most units. All of the dates from this initial suite yielded ages in the range of 1400–1600 radiocarbon years before present (ybp) (Table 2). These dates are in the same age range as four samples that we acquired from unit 5 in trench T9 and indicate that either the entire section was deposited in a very short period of time or that there was a source of carbon dating to that period that was incorporated into each of the units. A likely source of such carbon would be the burning of the forest by the indigenous people of the area to make way for agriculture or the intense occupation of a site upslope from trench T14 in the 1400–1600-ybp time frame.

To test whether the charcoal has been reworked into the deposits or whether the entire section was deposited over 200 years, we submitted a larger number of samples from the T14 site to see if young charcoal is mixed in with the 1400–1600-ybp group. The results in Table 2 show that all samples recovered from this site yield similar ages, although the youngest date (T14a-14) was recovered from the youngest unit (unit 2). We then ran two mean residency time (MRT) radiocarbon ages from the buried A horizons to test whether the soil ages were consistent with the detrital charcoal ages, which would indicate an older source for the detrital charcoal. In general, the MRT dates yielded slightly younger ages than the detrital charcoal but are still consistent with the detrital charcoal dates. These data suggest that the detrital charcoal ages are, in fact, a generally valid representation of the ages of the units.

Taking the youngest dates from each stratigraphic unit and assuming these are maximum ages for the host units

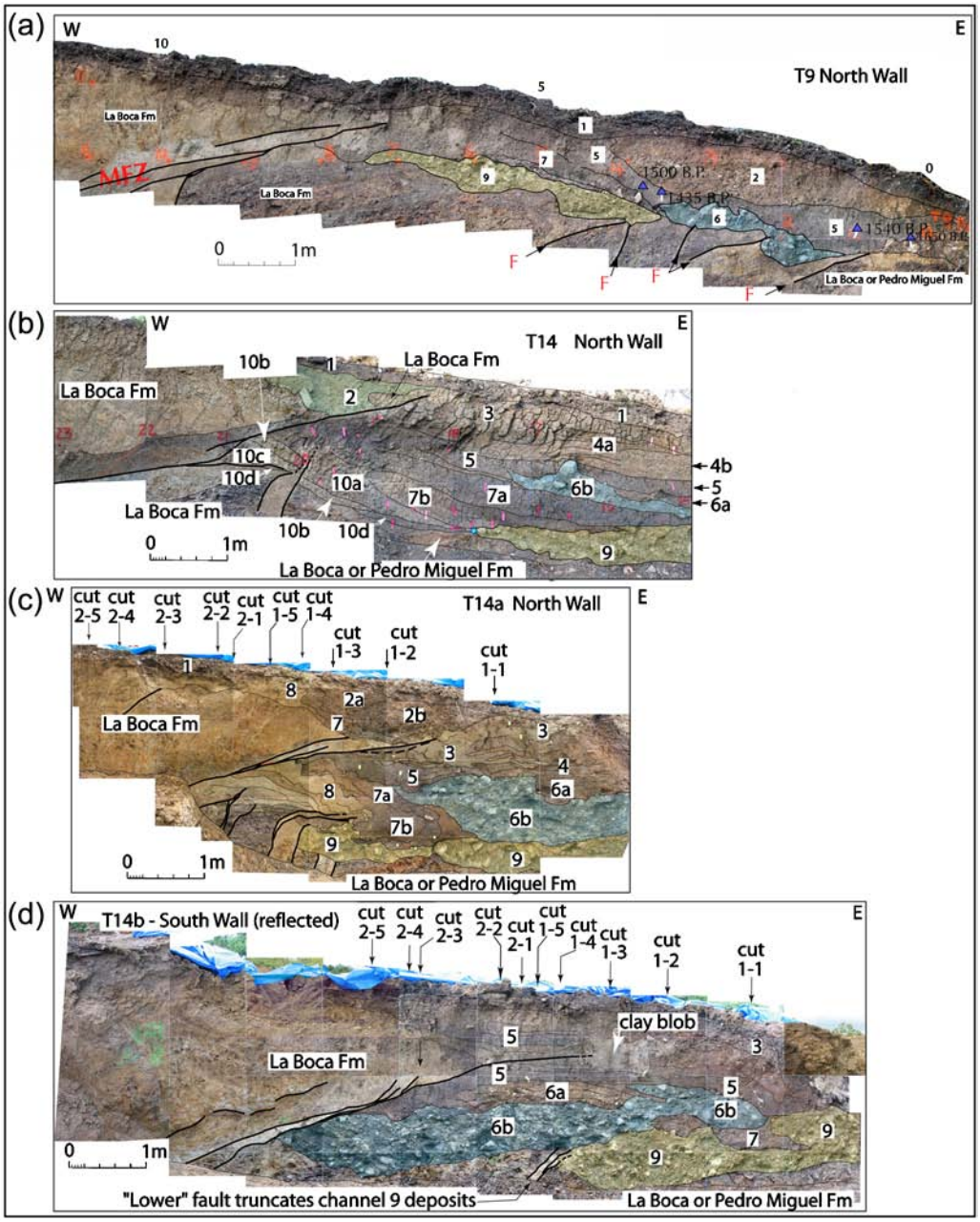

Figure 11. Logs of trenches T9, T14, T14a, and T14b (Fig. 8 and Fig. 10). Units are described in the text, as is the evidence for each faulting events. The locations of the slices (Fig. 13) are indicated where there intercept the faces of trenches T14a and T14b. The color version of this figure is available only in the electronic edition.

because they are all detrital charcoal, unit 2 is younger than AD 671–872, unit 3 is younger than AD 566–655, unit 7 is younger than AD 467–650, unit 8 is younger than AD 594–688, unit 9 is younger than AD 432–600, and unit 10d is younger than AD 396–547. The humic date from the unit 5 soil yielded an age range of AD 660–875, consistent with some residence age for the detrital charcoal but also arguing that the entire section is indeed about 1400–1600 radiocarbon years old.

Of the two OSL samples from trench T14a, one of them (OSL-T14a-1) is in complete agreement with the radiocarbon dating results, whereas the second one (OSL-T14a-2) yielded a date roughly twice as old as the radiocarbon age for the same unit. Apparently in this young channel, the partial bleaching of the quartz measured in the OSL dating may overestimate the OSL age by as much as 2000 years, which is inadequate for resolving the timing of past ruptures. Moreover, quartz grains were rare in the samples; and, because of the quartz stability problems we encountered with the older OSL dates, we did not use them to determine the ages of past ruptures, although they generally confirm the youthful nature of the section.

Table 2
Radiocarbon Dates and Their Calibrated and OSL Ages from Trenches at Cocoli on the Pedro Miguel Fault

Sample ID*	Unit ID†	CAMS# (LLNL Lab Number)	$d^{13}C$‡	^{14}C and OSL Ages‡	Calibrated Age (2σ)§
Trench T9 samples					
PM-T9-1	5	129344	−27.44	1415 ± 30	585 AD (95.4%) 663 AD
PM-T9-2	5	129345	−26.17	1530 ± 30	432 AD (95.4%) 600 AD
PM-T9-3	5	129346	−26.57	1635 ± 30	343 AD (95.4%) 534 AD
PM-T9-4	5	129347	−31.53	1445 ± 35	558 AD (95.4%) 655 AD
Trench T14, samples	T14a and T14b				
T14a-14	2	133758	−25	1255 ± 40	671 AD (95.4%) 872 AD
PM-T14-20	3a	130850	−25.30	1440 ± 30	566 AD (95.4%) 655 AD
T14-21	3a	134291	−25.04	1485 ± 25	467 AD (95.4%) 645 AD
T14a-3	upper 3	133750	−27.94	1505 ± 45	424 AD (95.4%) 616 AD
T14a-13	middle 3	133757	−25	1485 ± 35	443 AD (95.4%) 649 AD
T14a-4	3	133751	−21.46	> Modern	modern
PM-T14-5	lower 3b	130767	−24.92	1625 ± 30	353 AD (95.4%) 536 AD
T14a-7	lower 3	133753	−26.82	1505 ± 35	430 AD (95.4%) 617 AD
T14b-10	clay blob	133768	−25.87	1470 ± 30	535 AD (95.4%) 652 AD
T14b-11	clay blob	133769	−22.60	1565 ± 30	427 AD (95.4%) 593 AD
T14b-3	? 4/5	133761	−25	1455 ± 35	551 AD (95.4%) 651 AD
T14-3	upper 5	134294	−26.49	1405 ± 30	572 AD (95.4%) 663 AD
T14-3 ha	upper 5	134498	−25	1270 ± 50	660 AD (95.4% 875 AD
PM-T14-19	upper 5	130852	−26.12	1535 ± 30	419 AD (95.4%) 574 AD
T14-18	upper 5	134290	−29.19	1530 ± 35	417 AD (95.4%) 570 AD
T14a-5	5	133752	−25	1705 ± 40	245 AD (95.4%) 416 AD
T14a-8	5	133754	−25	1690 ± 40	249 AD (95.4%) 426 AD
T14b MRT-1	5	133861	−25	1480 ± 60	433 AD (95.4%) 656 AD
T14b MKT2	5	134288	−25	1435 ± 35	563 AD (95.4%) 658 AD
PM-T14-14	lower 5	130851	−25	1605 ± 35	388 AD (95.4%) 544 AD
T14-15 ha	5 to 7 contact	134500	−25	1420 ± 30	442 AD (95.4%) 766 AD
T14b-6	base 5	133764	−26.86	1485 ± 35	434 AD (95.4%) 644 AD
T14b-4	top 6/base 5	133762	−25.11	1785 ± 30	132 AD (95.4%) 338 AD
T14b-5	6b	133763	−25	2520 ± 130	970 BC (95.4%) 366 BC
PM-T14-2	upper 7a	130853	−26.18	1495 ± 20	540 AD (95.4%) 616 AD
PM-T14-6	7a	130854	−27.54	1525 ± 30	432 AD (95.4%) 604 AD
T14-23 ha	7	134501	−25	1480 ± 35	467 AD (95.4%) 650 AD
T14-23	7	134292	−26.90	1465 ± 30	467 AD (95.4%) 650 AD
T14a-2	7	133749	−27.08	1470 ± 30	441 AD (95.4%) 646 AD
T14a-9	7	133755	−27.34	1465 ± 35	438 AD (95.4%) 650 AD
T14b-7	7	133765	−27.98	1460 ± 30	443 AD (95.4) 649 AD
T14b-8	7	133766	−25	1510 ± 35	434 AD (95.4%) 635 AD
T14a-10	7	133756	−28.00	1535 ± 30	419 AD (95.4%) 574 AD
T14a-12	7a/7b	133774	−24.35	1945 ± 30	37 BC (95.4%) 130 AD
PM-T14-10	7b	130855	−24.55	1645 ± 35	263 AD (95.4%) 534 AD
PM-T14-12	top 8	130857	−28.77	1485 ± 30	455 AD (95.4%) 647 AD
PM-T14-4	8	130856	−26.06	1670 ± 30	258 AD (95.4%) 430 AD
T14-1	8	134296	−27.97	1390 ± 25	584 AD (95.4%) 663 AD
T14-1 ha	8	134497	−25	1700 ± 35	253 AD (95.4%) 415 AD
T14-7	lower 8	134295	−25.97	1510 ± 35	432 AD (95.4%) 623 AD
T14-7 ha	lower 8	134499	−25	1385 ± 35	594 AD (95.4%) 688 AD
T14-11	lower 8	134293	−21.49	1435 ± 30	580 AD (95.4%) 670 AD
PM-T14-13	9a	130858	−25	22060 ± 1100	Not calibrated
PM-T14-9	9a	130859	−13.00	1555 ± 30	424 AD (95.4%) 584 AD
T14a-1	top 9 gravel	133748	−23.44	1735 ± 35	242 AD (95.4%) 405 AD
T14a-15	9 gravel	133759	−27.03	1645 ± 25	258 AD (95.4%) 504 AD
PM-T14-8	9 gravel	130860	−25.91	1530 ± 25	432 AD (95.4%) 600 AD
PM-T14-16	10b	130861	−25.00	1595 ± 35	396 AD (95.4%) 547 AD
T14 OSL Samples					
OSL-T14a-1	2			1240 ± 110	
OSL-T14a-2	lower 3			3310 ± 270	
Trench T21 sample					
T21-LWC-1		133860	−25	175 ± 35	1660 AD (95.4%) 1954

(*continued*)

Table 2 (*Continued*)

Sample ID*	Unit ID†	CAMS# (LLNL Lab Number)	$d^{13}C$‡	^{14}C and OSL Ages‡	Calibrated Age (2σ)§
Trench T33 samples					
T33-MRT-4	Sta. 5.5 (−28–40 cm)	134299	−25	425 ± 35	1418 AD–1620 AD
T33-MRT-6	Sta. 6.9	134301	−17.28	2925 ± 25	1126 BC–926 BC
T21 OSL samples					
T21-HE1	ditch			2440 ± 220	
T21-BE	Ch. A			8520 ± 820	
T21-IE1 3D	Ch. C/D			6480 ± 710	
T21-IE2 3D	Ch. C/D			7050 ± 710	

*Samples with names that include T9 or T14 are from the T14 3D site. Ha refers to humic acid dates.
†The unit designations correspond to the logs of T9 and T14.
‡Some samples were run for ^{13}C, and the radiocarbon ages have been corrected accordingly.
§The calibrated ages are reported as the entire 2σ range and were calibrated in OxCAL (Bronk-Ramsey, 2005).

Identification of Past Surface Ruptures

We identified evidence for three separate surface ruptures that occurred in the past ~1600 years. We refer to these as events 1 through 3, with event 1 being the youngest. For this discussion, we refer to the main low-angle fault as fault 1 (Fig. 11). In the footwall of fault 1 are several higher-angle faults that we interpret to be transfer structures between surficial, low-angle fault petals, and these are collectively referred to as fault 2 (as a zone).

Event 1. Event 1 is obvious in all exposures and places the La Boca formation bedrock over soil and alluvium along fault 1. The fault can be traced in most exposures up into the surface soil units, appears to truncate the base of unit 2 in trenches T14 and T14a (Fig. 11b,c), and resulted in deposition of colluvium in the upper part of unit 3 (in this case, it is clear that the upper part of unit 3 must be younger than unit 2, but unit 3 was locally massive and a distinct event horizon was not possible to distinguish, so we could not delineate the pre-event and postevent components of unit 3 in most exposures away from fault 1).

In the T14 trenches, the age data only limit the occurrence of event 1 to younger than about 1300 years ago (sample 14 from unit 2 in T14a: AD 671–872), though it is likely much younger because the fault is well expressed up through the soil. Nevertheless, from the T14 trenches, the age data provide only a maximum date for this event as deposition had ceased at this site.

Event 2. Event 2 was initially interpreted in trench T14 from rupture of footwall fault 2, which displaces units 7–10 but could not be traced above the base of unit 7 (Fig. 11b). Furthermore, unit 7 itself appears to be a colluvial wedge complex that was generated by slip on fault 1, as the deposits thin and pinch away from the fault. We also debated whether the upper part of unit 7 represents a separate colluvial wedge and another event, although the subsequent exposure in trench T14a appears to have clarified this issue.

Trench T14a was cut only 50–70 cm north of the T14 exposure but revealed substantially enhanced clarity in the occurrence of event 2 (Fig. 11c). Fault 2 moved in this event and involved all units up through unit 7. The fault was observed to roll almost flat, folding unit 7 as a recumbent structure onto the gravel of unit 9, and this fold was subsequently buried by the undeformed gravel and colluvium of units 6 and 5. As is discussed further, we resolved displacement of unit 9 on fault 2 only; and, based on the generation of colluvium from fault 1 in this event, there was almost certainly movement on both faults in event 2.

Evidence for event 2 is also seen in trench T14b (Fig. 11d), where faulted gravels of unit 9 are overlain by unfaulted gravel of unit 6 along fault 2. Because most of the section between units 6 and 9 is eroded by the unit 6 gravel, this trench did not provide as good a resolution on the precise stratigraphic position of event 2, although it does support its occurrence.

The deformation associated with Event 2 is large and almost certainly coseismic. The event placed rock and soil a substantial distance over the unit 9 gravel, offset unit 9 a significant distance (as discussed subsequently), and is buried by undeformed units. These observations all argue that the deformation is not the result of creep but is due to slip in a very short period of time, as in an earthquake.

The event horizon for event 2 is bracketed by units 6 (AD 556–655) and unit 7 (AD 467–650), indicating that the age of event 2 is in the time frame of AD 640 (see more detailed discussion on the ages in the next section).

Event 3. Event 3 is inferred from the T14 exposure where the oldest part of the section is preserved. At the base of the section, unit 10d is a dark, organic-rich buried soil developed into the La Boca formation bedrock. A single piece of detrital charcoal was recovered from unit 10d on the east side of the fault in trench T14 that indicates this unit was buried no more than about 1600 years ago. This appears to have been the ground surface prior to deposition of the overlying section. At fault 1, a triangular-shaped block of probable La Boca

bedrock (unit 10c in T14, Fig. 11b) is juxtaposed over unit 10d and is, in turn, overlain by the wedge-shaped colluvium of units 10a and 10b. Event 3 is interpreted to postdate unit 10d, resulting in placement of rock on soil and subsequent deposition of a fault-derived colluvial wedge. Evidence for event 3 was not exposed in trench T14a, in spite of the close proximity of the two trenches (50–70 cm), as the gravel of unit 9 had apparently cut out the older section of unit 10.

In trench T14 (Fig. 11b), the precise relationship between event 3 and unit 9 is not clear. It is plausible that unit 9 predates the deposition of the colluvial wedge associated with event 3, as the colluvium of unit 10 and the gravel of unit 9 are at essentially the same level. If unit 9 is actually older than the upper part of unit 10, then our numbering system is a bit awry. The observation in T14 is that the unit 9 gravel ends at the toe of the unit 10 colluvium, and unit 7 overlies both. This is important when discussing the displacement of unit 9 and whether it is from one or two events. From our existing exposures, this relationship is not clear.

The timing of this event is bracketed by units 10d and 10a, but there are no age data for the colluvial wedge of unit 10a. Thus, we use the age data from unit 9 (AD 432–600) to place an upper bound constraint on the age of event 3 and that from 10d (AD 396–547) for the lower bound. Thus, these data place the event age at around AD 455.

To better constrain the event ages, we take the youngest dates from each unit and construct probability distributions for the event ages in OxCal (Ramsey, 2000; Bronk-Ramsey, 2001; Bronk-Ramsey, 2005), resulting in surface ruptures around AD 455, AD 640, and after AD 900 (Fig. 12). Using data from other trenches, the most recent event (MRE) must be historical (as discussed subsequently in this paper and in Earth Consultants International, 2007) and is likely the large historical earthquake of 1621. From this, and assuming that we did not miss an event, it is evident that earthquake recurrence has been irregular.

In summary, it is likely that there have been three surface ruptures on the Pedro Miguel fault in the past 1600 years, with the earlier two events well dated and the age of the most recent event poorly constrained from these exposures. We argue from dating from another trench (T33; Earth Consultants International, 2007), from the historical record, and from offset of the Camino de Cruces that event 1 is likely the large historical earthquake of 1621 that strongly damaged the original Panamá City (Panamá Viejo). If correct, then all three events occurred in a ~1200-year interval, which argues

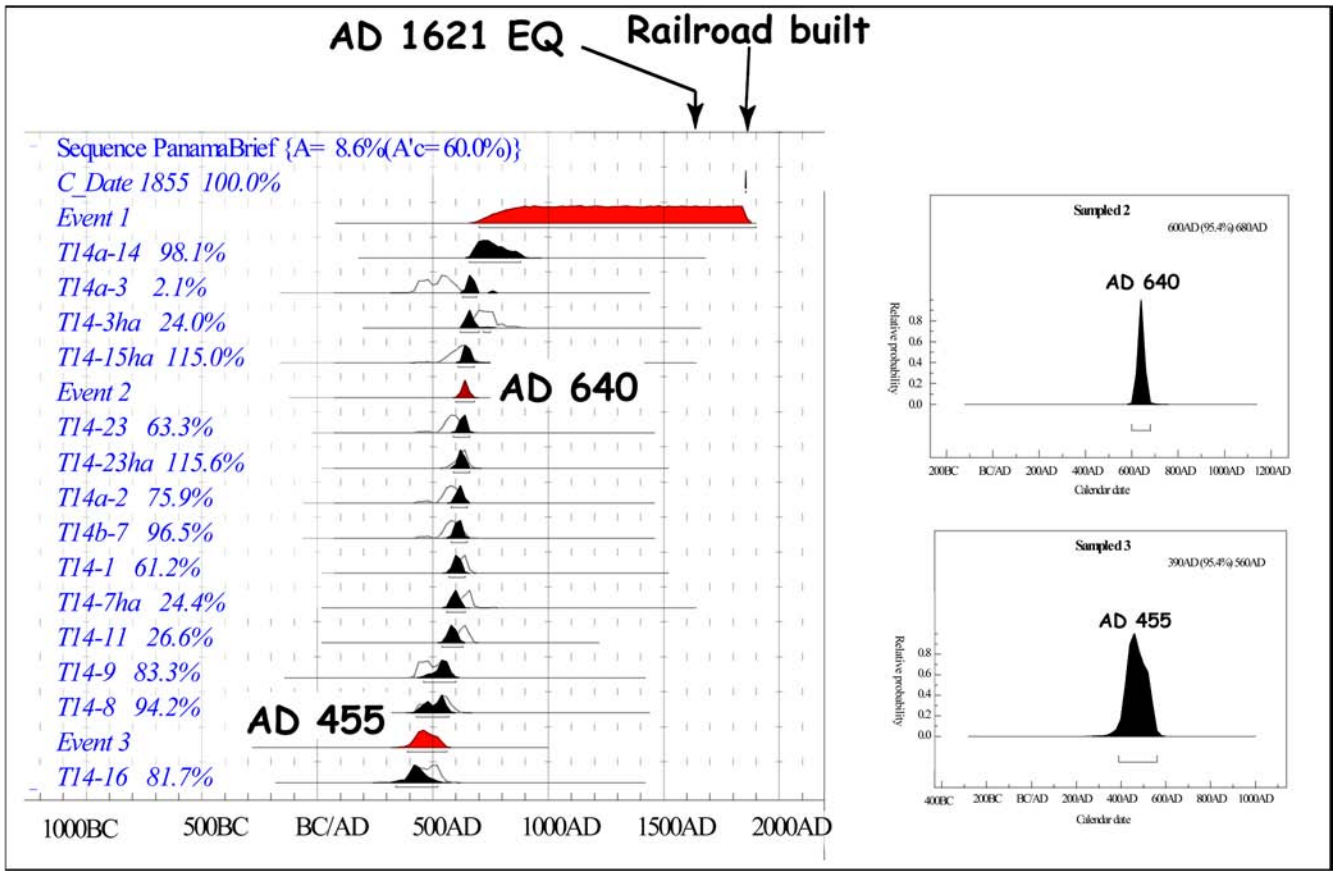

Figure 12. Probability distributions of the youngest radiocarbon dates from each unit. The event ages are plotted individually. Note that deposition at the T14 site apparently ended around 1200 years ago, so the most recent event(s) is poorly constrained in age. Atmospheric data from Reimer *et al.* (2004); OxCal v 3.10,Bronk-Ramsey (2005). The color version of this figure is available only in the electronic edition.

for a fairly short recurrence interval of about 600 years for the past 1600 years or so. These data also argue for irregular recurrence. We discuss the importance of this in the interpretation of the slip rate after we present evidence for slip per event.

Resolution of Slip

As part of this study, we tested the possibility of a preserved subsurface offset of channel units 6 and 9 by first excavating T14a about 0.5 m farther north from the T14 north wall with the intent to simply provide a fresh exposure (Fig. 10). The actual distance between T14 and T14a varied from about 50 cm in the western part of the new excavation to about 70 cm where the channels were exposed east of the fault. Surprisingly, the edge of the unit 9 channel had moved all the way to fault 2, where the channel gravel was now in fault contact (Fig. 11c), indicating that the gravel intersected the fault (the piercing point) on the east side of the fault somewhere between the two cuts. Although we inadvertently cut this piercing point out, we know its location to be within that 70-cm interval. For this exercise, we place the piercing contact for the unit 9 channel margin as halfway between the two walls and assign a ± 35 cm uncertainty to the location of the piercing point.

We then excavated trench T14b to explore the distribution of the channel deposits ~3 m to the north. This trench exposed La Boca bedrock juxtaposed over the unit 6 channel gravel along fault 1, with the unit 9 gravel in fault contact with fault 2. Thus, the eastern piercing point for the unit 6 channel was present somewhere between the trench faces of T14a and T14b. The unit 9 channel was found in fault contact in both exposures, so it must be offset more than the 3-m distance between the trench faces.

West of the fault, the south margin of the unit 6 gravel was exposed in the west end of trench T14b, and the gravel filled the north wall of T14b. (This relationship can be seen in Fig. 13, cut 2-1 which looks west—the feeder channel is located north of the north wall of trench face 14b, as mapped in Fig. 10). The location of the edge of the gravel was surveyed, and its position is known to within a half meter of where it intersects fault 1 on the west side of the fault. Thus, tracing the south margin of channel unit 6 into the fault from the east provides slip on fault 1 in the MRE, as fault 2 did not move in the MRE. Further, it provides a piercing point for the minimum displacement of channel unit 9, as the location of the unit 9 feeder channel cannot be any farther south than the unit 6 feeder channel because a fault-parallel trench we excavated on the west side of the fault did not expose another source for the gravel.

We then excavated a series of slices parallel to the fault to trace the margin of the unit 6 channel into the fault and to explore the distribution of other units. In all, ten slices were made (Fig. 10 and Fig. 13; eight interpreted photomosaic logs for cuts 1-1 through 2-5 are included in Fig. 13) that allowed for precise location of the unit 6 channel edge. These cuts also demonstrated that units 5 and 6a are the upper part of the same channel fill sequence for which unit 6b is the basal gravel.

For this exercise, we use the gravel of unit 6b as the primary piercing point, but we also note that the channel margin is seen to be offset a similar amount. Strike-slip was measured parallel to the average strike of the fault of N12E—not parallel to the low-angle faults that expressed oblique slip—because the direction of motion is oblique in the plane of the low-angle fault and there is a dip component of slip. Unit 6b was found to be offset about 2.1 m across fault 1. In cut 1-3 (Fig. 13), the top of the channel fill expresses a right-separation of about 1.8 m, and in cut 1-4 (Fig. 13), the right separation is as much as 2.4 m. Taken together, and considering that our uncertainty on the precise location of the gravel channel west of the fault is about a half meter, we assign 2.1 ± 0.5 m for the minimum slip in the MRE. It is a minimum because we cannot discount the probability that some warping occurred on the hanging wall on this low-angle fault or that other vertical strands (similar to fault 2, which we interpret as a step-over transfer structure) in the hanging wall may have accrued some slip. In trenches T9 and T14, we noted several minor faults in the hanging wall that displaced the topsoil, supporting this argument.

The additional cuts confirmed the continuous presence of the unit 9 gravel in contact with fault 2 between the faces of T14a and T14b, yielding an absolute minimum displacement of 3 m, none of which occurred in the MRE because fault 2 did not slip in the MRE. If the feeder channel continued along its trend across fault 1 to fault 2 (an additional 5 m at the elevation of the unit 9 channel gravel), then we infer about 4.5 m of post-unit 9 displacement (Fig. 10). An alternative method is to sum the minimum slip values from Fault 1 in the MRE (2.1 ± 0.5 m) and fault 2 (minimum of 3.0 ± 0.35 m) in the penultimate event, in which case the unit 9 channel is offset at least 5.1 ± 0.85 m. However, based on the observation in trenches T14 and T14a that fault 1 also likely moved when the unit 9 channel was displaced (presence of a colluvial wedge shed from fault 1 in the penultimate event), this displacement value is a gross minimum. Thus, after deposition of unit 9, there has been at least ~5 m of lateral slip, with the likelihood that the actual displacement is larger. Because of the uncertainty between the age of deposition of unit 9 and the occurrence of event 3, it is plausible that this large displacement occurred in three events. However, from the T14 exposures, we cannot preclude that the displacement in the penultimate event (event 2) was substantially larger than that which occurred in the MRE (event 1).

In summary, we have resolved a minimum displacement of 2.1 ± 0.5 m for the gravel of unit 6, which can only be attributed to event 1. For unit 9, we have resolved a minimum additional displacement of 3 m, which is likely the result of event 2. As discussed previously in this paper, there was also additional slip on fault 1 during event 2 that resulted in the colluvial wedge of unit 7. Thus, it appears that event 2 was

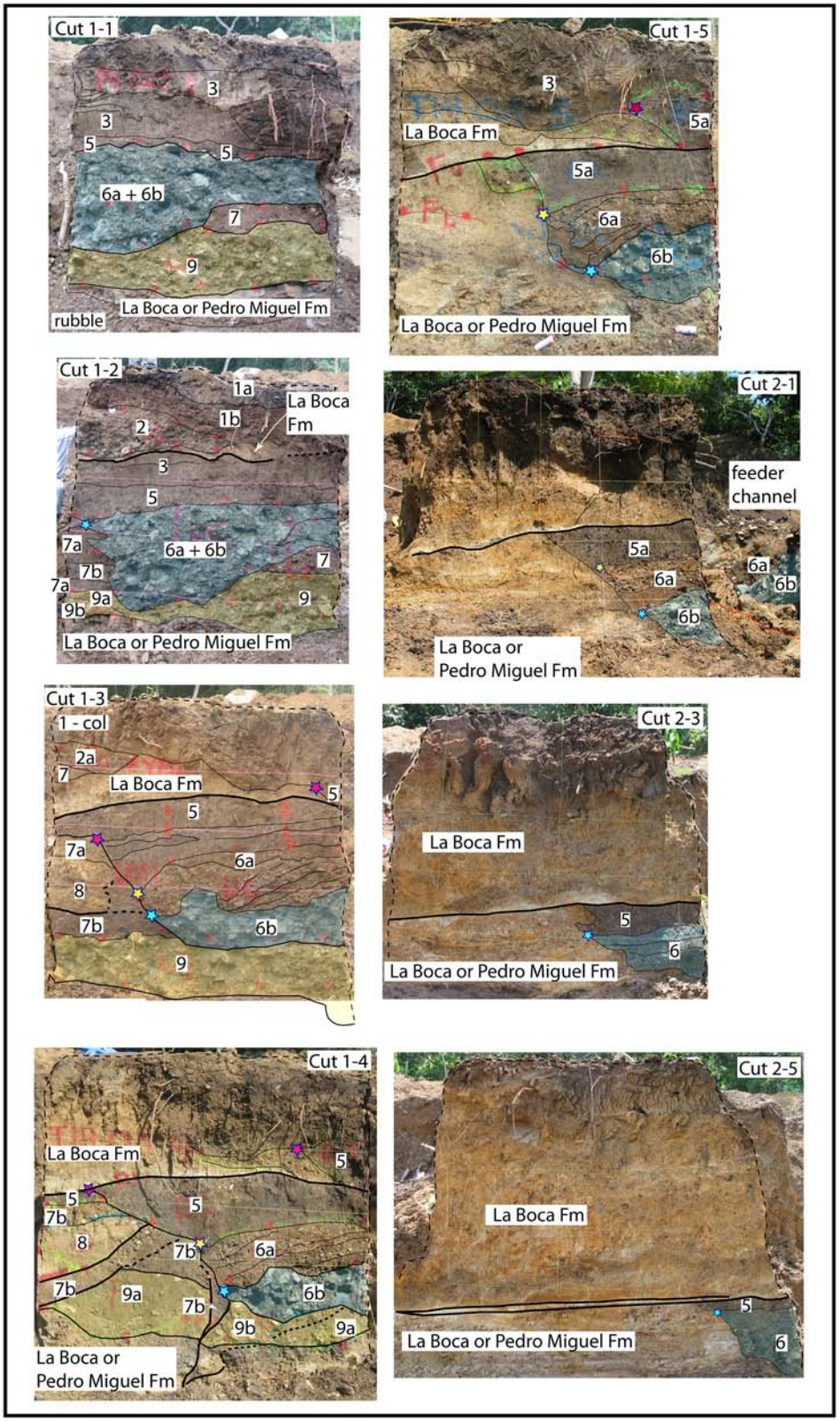

Figure 13. Slices of the block of soil between trenches T14a and T14b. The location of the slices are shown on Figures 10 and 11. Note the location of the unit 6 and 9 gravels as each slice is cut progressively into and across the faults. The main, low-angle fault is seen as the nearly horizontal bold line across each of the exposures. The color version of this figure is available only in the electronic edition.

larger than event 1. However, because of the uncertain relationship in the age of units 10a and 9, we cannot preclude that some of the displacement associated with unit 9 occurred during event 3.

Timing and Displacement of Buried Channels at the Trench T21 Site

The excavation of trench T21 (Fig. 8) initially was conducted to resolve the location of the Pedro Miguel fault and to test whether a ~2.5–3-m deflection of a surface channel was potentially fault related. Unfortunately, this particular geomorphic feature was inadvertently destroyed during grading for vegetation removal before we could get it surveyed, but it was very similar to the 2.6–3^{+}-m stream-wall offset that is still visible in the adjacent drainage, located 50 m north of trench T21 (Earth Consultants International, 2007).

Trench T21 exposed a channel filled with a distinct, light-colored gravel offset by a west-dipping, low-angle fault (Fig. 14). The distribution of gravel exposed in the trench walls, herein named channel A, required the presence of lateral slip, confirming the geomorphic offset and making this an attractive site to explore the kinematics of the fault in three dimensions.

Therefore, after initial logging of trench T21, we cut a number of new trenches oriented more or less parallel to the fault zone and perpendicular to the original trench T21 (labeled trenches T21A through T21L on Fig. 15). In particular, we were interested in resolving the lateral distribution of the channel A gravel, exposing other channels that, if present, might provide useful information on the fault's Quaternary displacement and improve our understanding the three-dimensional character of the fault zone.

Channel A and the Feeder Channel

West of the fault, we exposed the feeder channel in three trenches (T21A, T21B, and T21C), which, taken together, show that the channel bends to the right (south) as it approaches the fault in the far field. Two meters west of the fault, the channel bends back to being nearly perpendicular to the fault, which is opposite the sense expected for lateral drag. The feeder channel is not only the source for channel A but also for several other channels exposed in the lateral trenches, as discussed subsequently.

East of the fault, the margins of channel A were exposed in a sequence of trenches excavated parallel to the fault (Fig. 15), with a small, 4-inch-wide (~10.2-cm) slot trench at the fault demonstrating the precise location of the southern channel margin, which we use as a piercing point. However, the southern margin of the feeder channel on the west side of the fault was cut out in the initial excavation of T21, so there is an uncertainty equal to the width of the inner trench cut of T21 (~1 m) as to the precise amount of displacement on this piercing point.

Figure 15 shows the distribution of the channel A gravel (including the feeder channel gravel) as it approaches and crosses the fault. The northern margin is well preserved and is offset about 1.7 m. However, it would have been expected that this margin would have been trimmed by additional flow if the channel was active at the time of displacement. The southern margin is precisely known east of the fault, but to the west it was cut out in the initial excava-

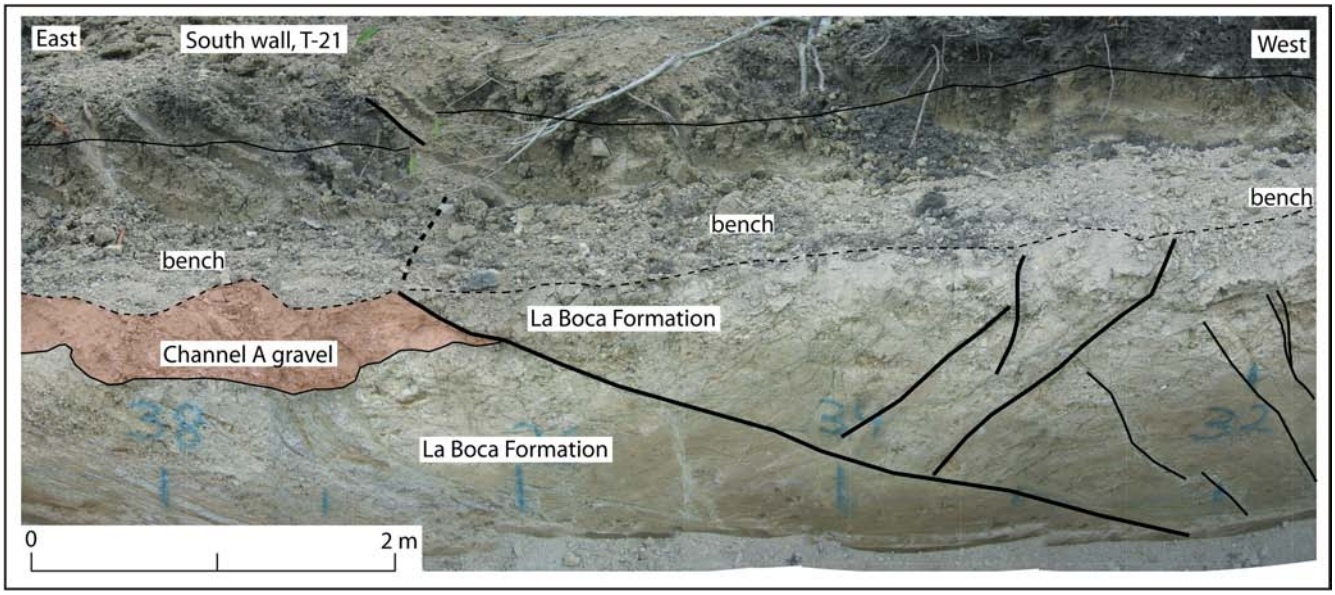

Figure 14. Annotated photomosaic of the south wall of trench T21 (prior to excavation of the 3D trenches; see Fig. 8 for location). Channel A is exposed in the trench face only east of the fault, making this interesting for a 3D excavation. The color version of this figure is available only in the electronic edition.

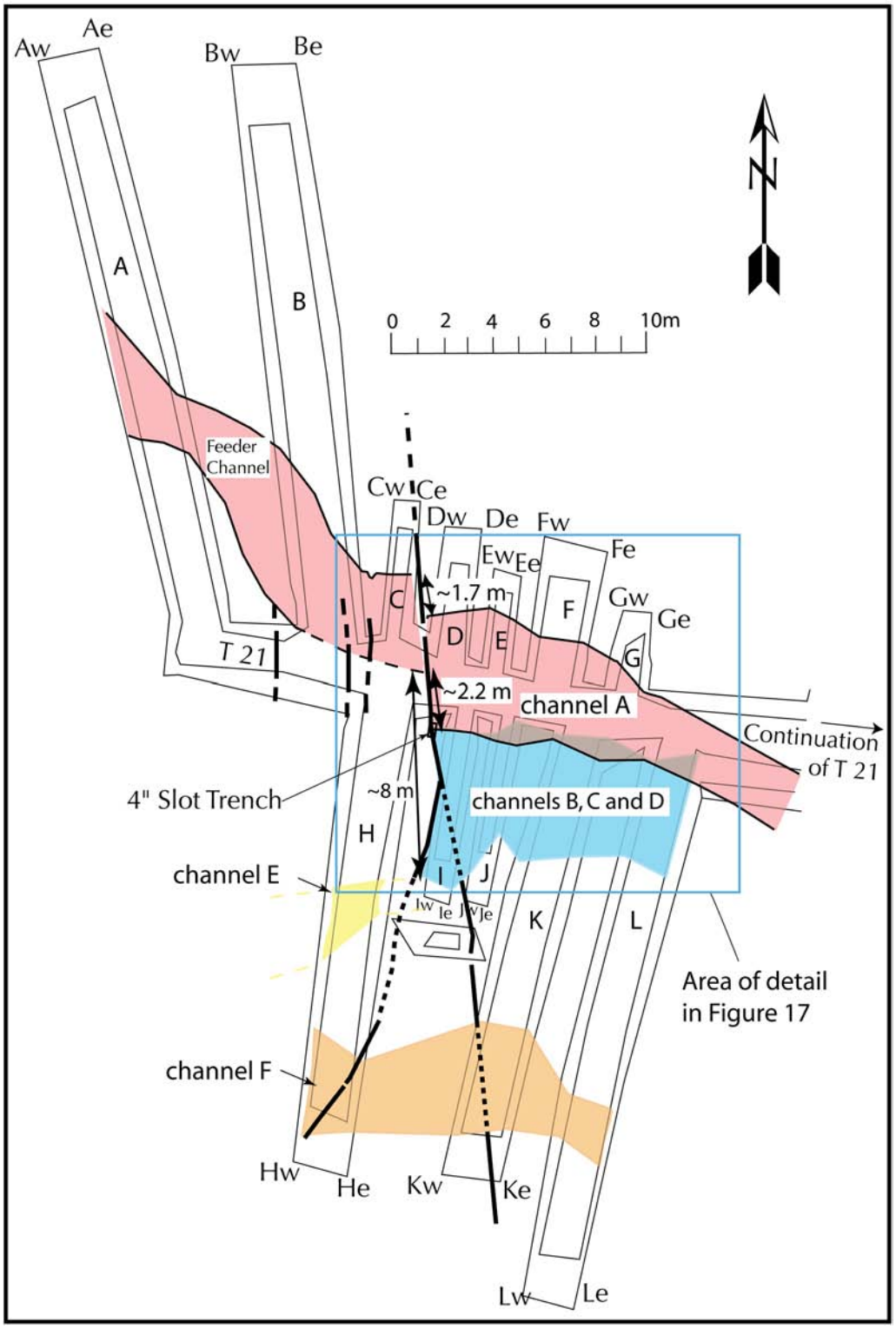

Figure 15. Map of 3D trenches at the T21 site (see Fig. 8), along with generalized locations of major channel elements. The ancillary trenches are labeled A through L, with the east and west walls noted by the lower case w or e. Note that the trench walls were sloped, so there is an upper and lower edge indicated for each trench. The color version of this figure is available only in the electronic edition.

tion of T21, as previously mentioned. For the southern margin of the feeder channel, we place the location in the middle of T21 and assign an uncertainty that is equal to half the width of the inner trench slot cut (about 1 m). Using this location, we estimate the southern margin to be offset 2.2 ± 1 m across the main fault, similar to the northern margin.

In addition to the main fault trace, these trenches exposed several secondary faults that, as in the T14 area, seem to be transferring slip between the low-angle primary structures. At least one of these hanging-wall faults cuts the feeder channel gravels and part of the deflection west of the fault on the hanging wall could be attributed to lateral warping, so displacement along the primary fault must be assumed to be a minimum. The channel wall of a small gully, located about 25 m north of trench T21, was measured to be offset 2.6–2.8 m at the fault, and this likely provides a reasonable estimate of the actual displacement in the most recent event.

Offset of Channels B, C, and D

South of trench T21, the fault-parallel trenches on the east side of the fault exposed a complex of nested channels south of channel A, which we herein name channels B, C, and D, respectively, in succession southward. The channels are best seen as separate features in the logs of lateral trenches I and J (Fig. 16) but are grouped together in Figure 15. In all exposures where each channel is preserved, the stratigraphic relationships between the channels show that channel D is oldest and channel B is youngest. Furthermore, there is a general pattern of lowering of the thalweg elevation from the oldest (D) to the youngest (B) channel, indicating long-term incision during the cutting and accumulation of the deposits associated with these channel forms.

Channels D and C have gravelly sand at their bases, with scattered cobbles up to 15 cm in size. The gravelly sand layer is generally capped by fine-grained alluvium or colluvium, some of which displays bedding. In contrast, channel B is filled with massive clayey silt and generally lacks gravel, indicating a change in hydraulic conditions between the filling of channels C and B. Channel A, as discussed earlier, is gravelly sand and represents a return to conditions inferred to have been similar to the cutting and filling of channels D and C.

We traced each of the channels and their deposits from trench face to trench face (Fig. 16 and Fig. 17). In the detailed map of the trenches and channels (Fig. 17), the trenches are indicated by an inner (base) and outer (top) line because most of the trench faces had some slope and because the surveyors tended to survey the base of the trench somewhat inside the actual base of the trench face. The critical channel contacts, however, were directly surveyed, so they appear about midway between the top and bottom of the surveyed trench locations because the channels were located midway up the trench faces.

As seen in Figure 16 and Figure 17, the B/C/D channel complex is abruptly truncated by the fault zone, and there is no equivalent channel complex preserved in trench H west of the fault. We did, however, observe another channel in trench H located south of the projection of the B/C/D channel complex, and there was concern that perhaps this channel (channel E, Fig. 15) somehow fed to the channel complex east of the fault. To test this, we excavated a number of destructive cuts through the block between trenches H and I and determined that (1) the B/C/D channel complex is abruptly truncated at a high-angle fault that roots into the low-angle main fault exposed in trench T21 and (2) there are no gravel or other channel deposits obscured in that block by which the channel E could have fed to the B/C/D channel complex without left-lateral slip. Because we are certain of the direction of slip on the youngest channel (right-lateral), we are confident that this possibility is highly unlikely and we discount it. From this exploration, we infer that channels B, C, and D all originated from the same feeder channel as channel A, although not necessarily with the same width and depth configuration as channel A.

Figure 18 shows a series of three reconstructions that assume all of the channel deposits originated from the feeder channel. In the first reconstruction, we back-slip the fault and align channel A directly in front of the feeder channel, using an average of 1.9 m based on the 1.7 and 2.1 m offsets resolved from the north and south channel margins, respectively. As previously discussed, this 1.9-m reconstruction probably underestimates the actual displacement because the southern margin is slipped into a protective position and should be better preserved, whereas the northern margin is subject to continued erosion. Thus, the southern margin reconstruction of about 2.1 m (with the attendant uncertainties) is a better estimate.

For channel B, we realign its southern margin to resolve about 4.6 m of displacement. The northern margin of channel B has been cut out by channel A, so this is the only estimate of displacement available to us. (Note that we are correlating to the closest channel margin and not to the preserved deposits because the feeder channel is filled with gravel that is clearly younger than the mud that fills channel B. Nevertheless, subtracting the 1.7–3.6 m displacement of channel A from the ~4.6 m displacement of channel B results in a reasonable minimum estimate of displacement on the main fault for the penultimate event of about 1–3 m.

Reconstruction of channels C and D requires additional interpretation. It is uncertain as to whether channels C and D represent a channel complex that was offset by a single earlier event (event 3, counting back from the youngest displacement event that offsets channel A) or whether each channel represents offset in two separate discrete events (events 3 and 4). The problem is twofold. First, the stratigraphy in all exposures demonstrates that channel C is cut into and is slightly lower than channel D and is therefore younger. It is also closer to the feeder channel, so it can be inferred to represent an additional event. However, channels D and C are, on their own, considerably narrower than the feeder channel; and, if they represent individual events, then the feeder channel itself must have grown in width in the time since the cutting of channel D. This is possible, and we note that channel D is both the narrowest and topographically highest of the channels, whereas channel A is the lowest (or nearly so) and the widest. This could represent the growth of a rill into a small channel over time, during which as many

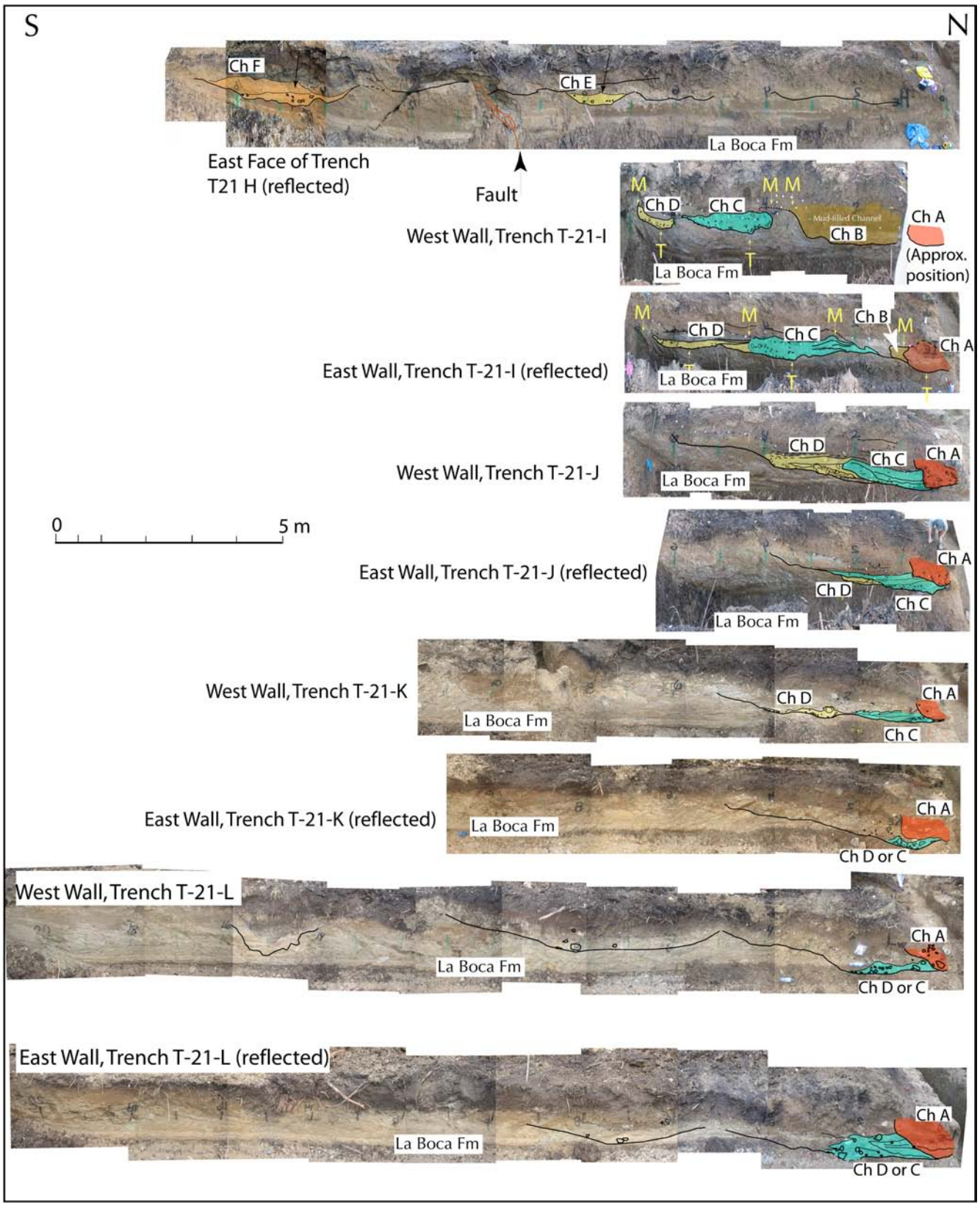

Figure 16. Logs of ancillary trenches H through L at the T21 site (Fig. 15). Note the locations of channel elements B, C, and D, which are used to map out their distribution and resolve lateral displacement. The color version of this figure is available only in the electronic edition.

as four earthquakes produced slip on the Pedro Miguel fault. Alternatively, channels C and D are collectively as broad as the feeder channel and could represent a nested channel sequence that was offset from a similar-sized feeder channel. In this scenario, there have been only three events that have occurred since the cutting of channel D.

The primary difference in interpretation reflects the inferred size of event 3 (or events 3 and 4). In panel C of Figure 18, we reconstruct channels D and C to the feeder channel to resolve about 8.1 m of displacement. We chose this representation because these two channels are collectively about the same size as the feeder channel. If this representation is correct, then there have been only three events, and the oldest of these events was apparently larger, with nearly 3.5 m (8.1–4.6) of slip on the main fault. Alternatively, if there have actually been four events since the deposition of channel D, then the average displacement per event for all four earthquakes is about 2 m, similar to that resolved for channel A, and argues for fairly characteristic slip. The actual displacement across the entire fault zone is likely more, based on our geomorphic observations of small channel offsets in the Cocolí area, as well as the observation that other secondary faults displace the feeder channel deposits in the hanging wall of the fault.

Other Channels

As noted previously, channel E is present west of the fault but has no match east of the fault that we identified. It is likely that the offset portion of channel E is located farther south along the fault, but we did not explore for this because we found no charcoal in this channel. Finally, there is a colluvium-filled channel farther south that we investigated (channel F in Figure 15). The channel is not faulted in

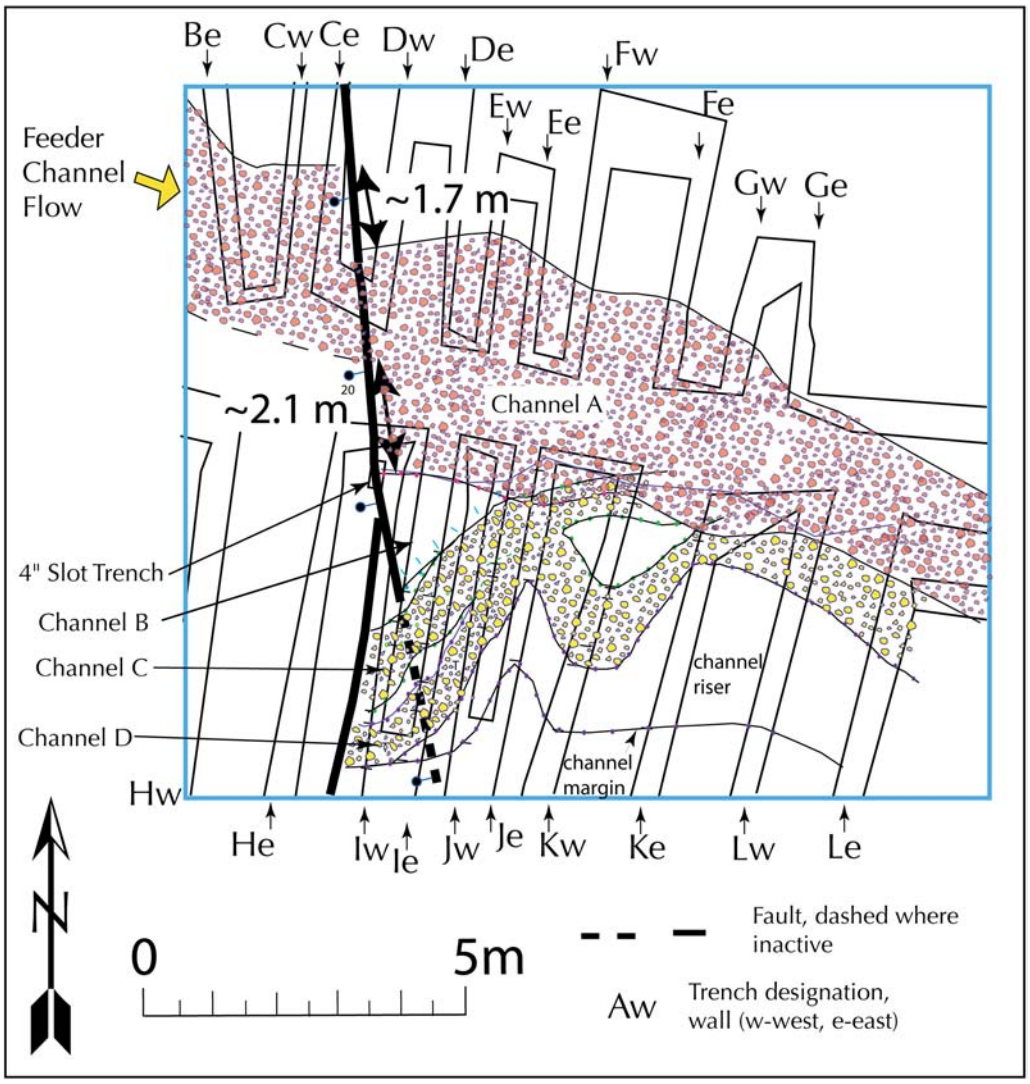

Figure 17. Detail of the distribution of gravels and channels at the T21 site. The displacement for each channel element is discussed in the text. The color version of this figure is available only in the electronic edition.

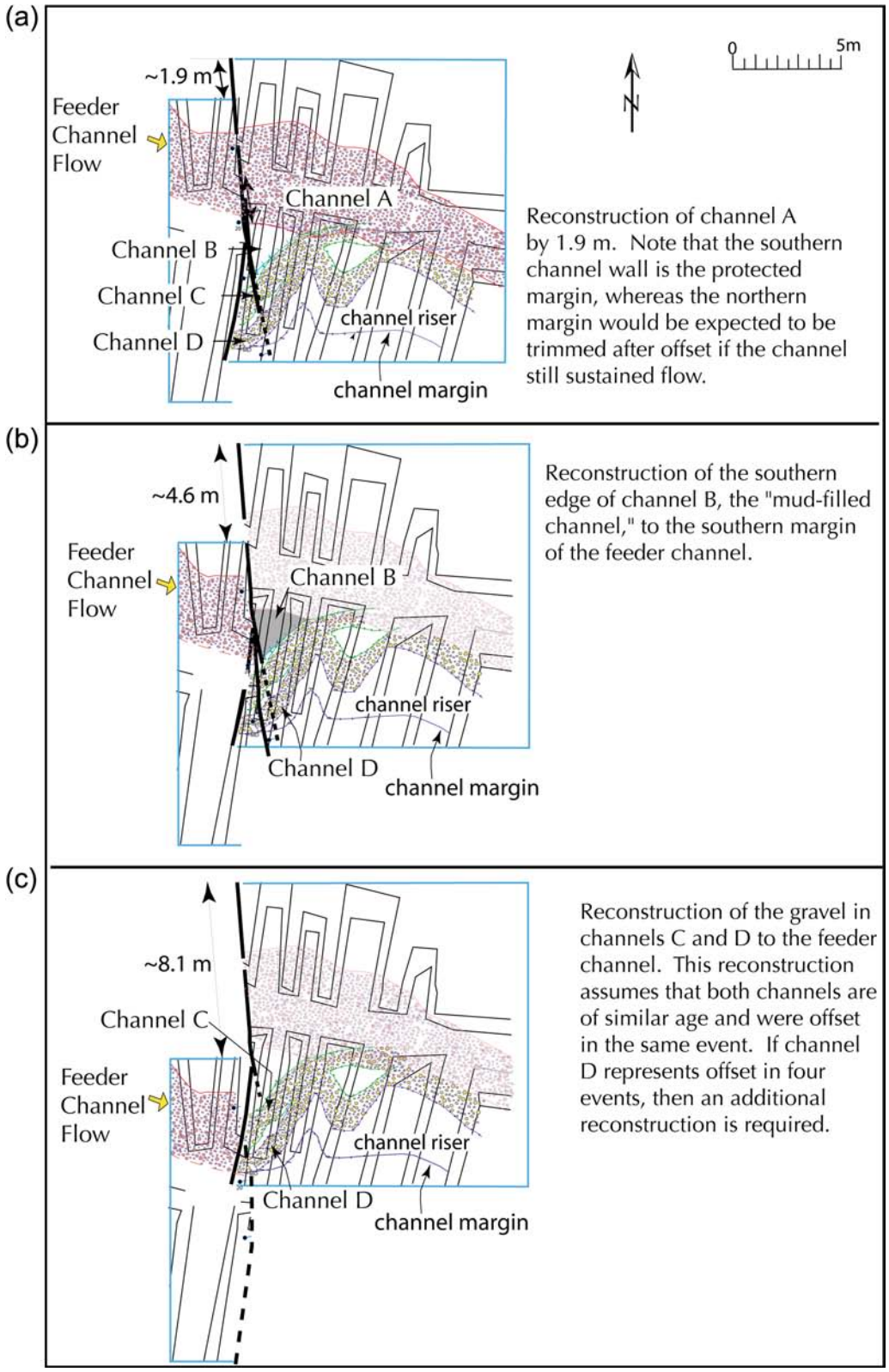

Figure 18. Reconstructions of offset channels at the T21 site. See text for discussion on these reconstructions. The color version of this figure is available only in the electronic edition.

any exposure, and the channel form appears to trend across the fault with no offset. In fact, this channel is a narrow, deep rill filled with colluvium and may in fact be a historical drainage ditch. In any case, we could find no charcoal in this channel, but it was sampled for OSL, which yielded a ~2.5 ka date, as is discussed subsequently. Presumably, the channel is

very young and postdates the MRE in spite of its apparent OSL age.

Age Control

Age control for the trench T21 stratigraphy is very poor. We found only three pieces of detrital charcoal, and two of these did not produce sufficient carbon to yield results. The third sample that did yield a date was interpreted to be detrital charcoal and was recovered from the channel C alluvium into which channel A is incised. Thus, it must predate the most recent event. This sample (T21-Lw C-1) yielded a date of 175 ± 35 radiocarbon years before present, which dendrocorrects to a calendar date that is younger than AD 1660. This is problematic from two perspectives. First, it makes the most recent event on the Pedro Miguel fault not only historical but too young to correspond to the large 1621 earthquake. Other more recent earthquakes that are reported in the literature include a poorly documented earthquake on 11 January 1849 that reportedly collapsed stone buildings in Panamá City; an earthquake on 25 April 1855 that was felt in Panamá City, Gatún, and Aspinwall (Colón), and the 13 October 1873 earthquake that was felt both in Panamá City and Colón. Though improbable, we cannot preclude that this event was associated with an aftershock to the great 1882 earthquake that is thought to have occurred on the north Panamá deformed belt.

Alternatively, we may have misidentified the charcoal in the field such that what we dated was actually a burned or carbonized root. Because we have only a single date, this is a very difficult issue to resolve without further work and dating. To address this, we collected OSL samples from the sediments of channels A and D, as well as from the younger, colluvium-filled channel that is not apparently displaced by the fault. The sample from the young colluvium in channel E (T21-HE1), which is likely historical and may fill a drainage ditch, yielded an OSL age of 2.44 ± 0.22 ka. The sample from channel A (T21-BE) yielded an age of 8.52 ± 0.82 ka, which taken at face value would suggest only a single surface rupture in over 8000 years; this is known to be incorrect from the event chronology recorded in the T14 site, as discussed earlier in this paper. Finally, two samples were recovered from the channel C/D deposits (samples T21-IE1 3D and T21 IE2 3D) that yielded ages of 6.48 ± 0.71 ka and 7.05 ± 0.71 ka, respectively. Based on stratigraphic relationships, the deposits that yielded these two samples must be older than the deposits that fill channel A, which yielded the ~8.5 ka date. From the known relative ages, it appears that there are substantial bleaching problems in the rare quartz in the OSL samples that we collected from the T21 site, making their use problematic in precise dating of the sediments in these trenches.

Two last pieces of age evidence are noteworthy from the T21 complex: none of the deposits are very weathered, and there are no saprolitic soils developed in any of the alluvial units. Based on visual comparison to the soils at the T14 site, where we have abundant age control, the T21 soils look similar and are probably in the same general age range. In contrast along the Gatún fault, the soil developed in the radiocarbon-dated 2.5–3.3-ka alluvium (Earth Consultants International, 2005) appears stronger, with a reddened argillic horizon. From this general comparison, we infer all of the deposits in channels A through D to be Late Holocene in age and likely younger than 2.5 ka.

Offset of Camino de Cruces

The Camino de Cruces is a 1.5-m-wide cobblestone (paved) road that was first established circa 1533 to enable large mule pack trains to move Incan gold across the isthmus (Fig. 2). The original track extended from the old town site of Panamá Viejo (near modern Panamá City) on the Pacific coast, across the drainage divide, to the town of Cruces on the Chagres River, approximately across from the present town of Gamboa (Fig. 2). It was in nearly continuous use until completion of the railroad in 1855, after which the trail was abandoned.

During the course of our investigations, several observations suggested that the most recent rupture on the Pedro Miguel fault may have been fairly recent and possibly historical in age. In addition to the problematic very young age of carbon in faulted alluvium from the T21 offset channels, a radiocarbon date on charcoal from a soil beneath bedrock in T33 (Fig. 8) indicated faulting in the past several hundred years. Furthermore, several small channel deflections that we interpret as rill offsets appear fresh and young, with apparent displacements in the 2.5–3-m range. Based on these observations, we (T. Rockwell, and E. Gath, together with W. Lettis, and D. Ostenaa) walked the reach of the Camino de Cruces near the northern mapped trace of the fault to search for its intersection with the fault (see Fig. 2 for general location). Using a handheld GPS receiver, we followed the trail to the vicinity of the fault crossing as mapped by Stewart *et al.* (1980) and found an apparent ~3 m right-lateral offset of the trail and an associated low scarp across the lowest fluvial terrace near the confluence of two small drainages. Aligned with this offset, the modern stream channel walls and the riser above the low terrace are also deflected about 3 m, whereas the modern stream channel itself is diverted right-laterally over 30 m, forming a horseshoe-shaped meander. Other geomorphic features typically associated with active strike-slip faults were observed to the north, on trend with the fault (Earth Consultants International, 2008).

ACP's Topographic, Hydrographic, and Cartographic Section of the Engineering Division conducted a detailed topographic survey of the area (Fig. 19), which allowed us to analyze the geomorphic characteristics of the site and quantify the trail deflection. In addition to topography, the survey team located the edges of the deflected streams, the thalwegs of deflected rills, and several other important geomorphic features that were identified by our group. They also surveyed the location of hundreds of clasts along the old roadbed of the Camino de Cruces and the three trenches that

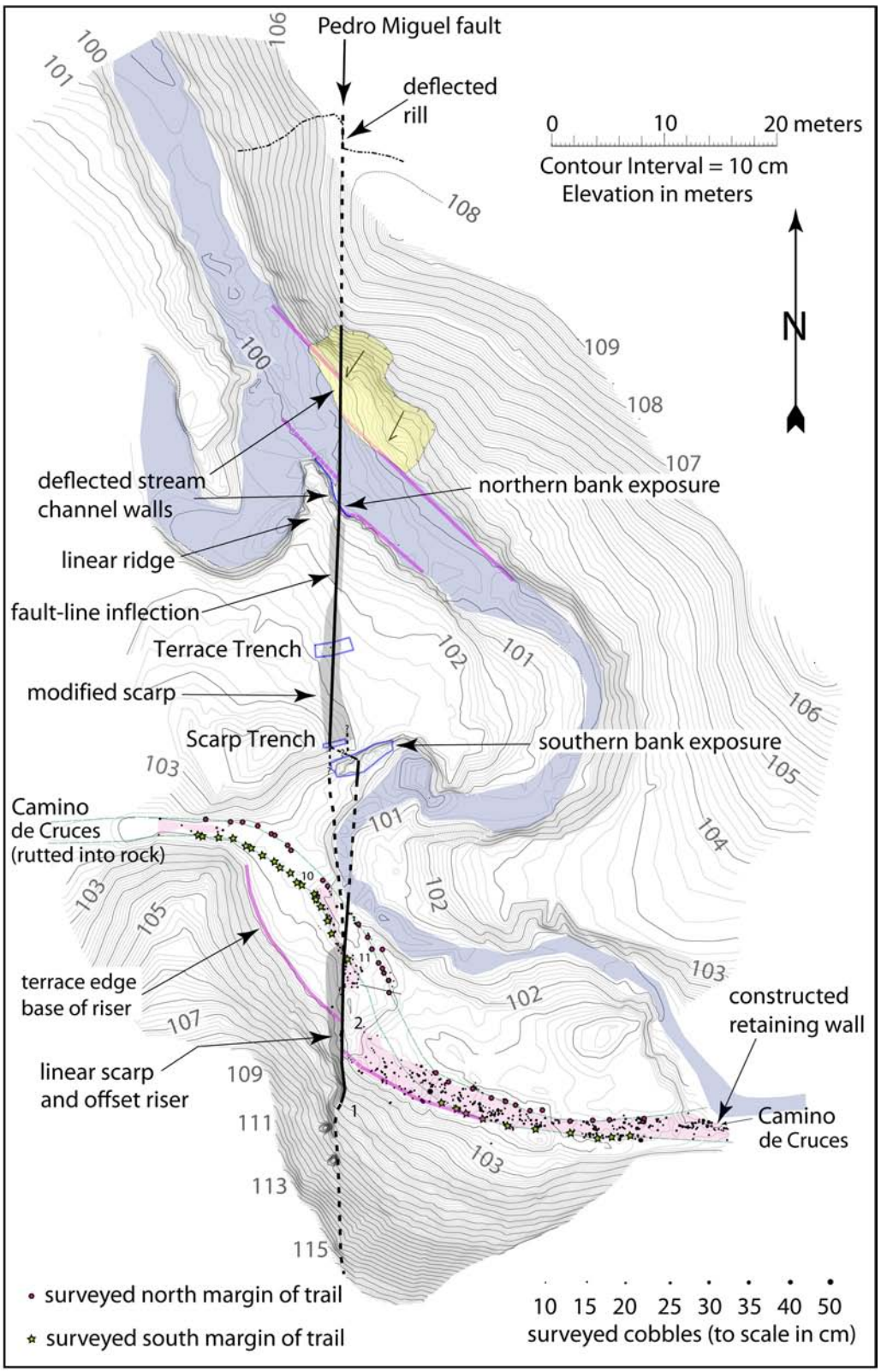

Figure 19. Annotated topographic map of the Camino de Cruces trail crossing the Pedro Miguel fault. Note the several offset rills, channel margins, and riser along with the offset of the trail itself. Note also the location of the trench and stream bank exposures used to confirm the location of the main fault. The cobbles of the trail were individually surveyed and categorized by size. The color version of this figure is available only in the electronic edition.

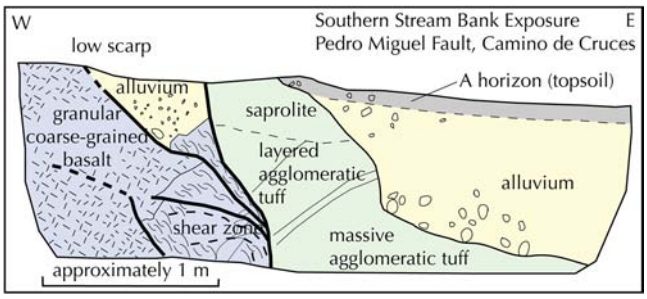

Figure 20. Trench log of the hand-excavated southern stream bank exposure across the Pedro Miguel fault near the Camino de Cruces trail. See location of this exposure on Figure 18. The color version of this figure is available only in the electronic edition.

we had hand-excavated across the fault zone. This allowed us to map out and reconstruct the trail to resolve displacement across the fault.

The three small trenches and two hand-cleared stream-cut exposures into the low terrace to the small creek exposed the fault in Late Holocene alluvium (Fig. 19 and Fig. 20). The trenches confirmed that the fault is spatially associated with the trail deflection and the various observed geomorphic offsets. We infer the alluvium to be Late Holocene because it expresses a low degree of weathering (essentially none) similar to other Late Holocene sites that we directly dated by radiocarbon on detrital charcoal. However, we found no charcoal in any of the trenches, so we have no direct dates on the low terrace itself.

The simplest reconstruction is to find the amount of retrodeformation that best matches all of the deflected and offset features (Fig. 21). The trail itself curves as it crosses the fault, in part because the trail hugs the edge of the low terrace south of the fault but aligns with a constructed cut in rock as the road climbs out of the terrace to the west of the fault. Thus, the overall trail deflection is greater than the actual trail offset. However, the configuration of the original roadbed has a very sharp deflection at the fault and it is highly unlikely that the road was built that way, considering the volume of traffic. The trail appears to have been rebuilt or straightened across the fault after the offset because we mapped remnants of the trail divergence east of the fault, with one trail truncated at the fault and the other aligned with the trail portion heading for the bedrock notch. Considering all of the deflected and offset features, a reconstruction of about 2.8 m realigns the four well-defined piercing lines, suggesting this is the actual displacement from the most recent event. We assign an uncertainty of about 0.5 m to this offset as the overall misfit to the four features.

These observations require the Pedro Miguel fault to have ruptured historically, between the trail's completion around 1533 and its abandonment in 1855. There is only one well-documented earthquake in this time frame, the 2 May 1621 earthquake, that appears to have been sufficiently large to have produce 2.8 m of displacement, and we thus attribute the offset of the Camino de Cruces to this earthquake.

The 1621 Earthquake

Based on the description of the main shock by Salcedo (1640), shaking was so intense in Panamá Viejo that it was difficult to maintain equilibrium. Strong aftershocks continued throughout the evening and for at least 24–48 hours afterwards, with four to five aftershocks felt every hour. Peraldo and Montero (1999) interpret Salcedo's description of the stronger of these to suggest that the seismic waves were observable at the ground surface. For at least 15 days following the mainshock, there were three to four aftershocks every day, so people feared entering their houses. Aftershocks continued, although diminished in number and strength, for three-and-a-half months, until 21 August. The earthquake resulted in extensive damage or collapse of the stone and adobe structures in Panamá Viejo, which is consistent with a modified Mercalli intensity of at least VIII. Based on the damage alone, reported from a single locality, it is not possible to estimate earthquake magnitude, but the reported damage is compatible with an earthquake close to M 7, which is also consistent with the observed offsets at Camino de Cruzes.

Discussion

Our paleoseismic work on the Limón and Pedro Miguel faults demonstrates that these are active, seismically capable faults that have ruptured during the historical period. They have a relatively short return period for large earthquakes, with displacements in the range of 1.5–3 m. Consequently, they represent a major potential seismic hazard to central Panama and specifically to Panama City and the Panama Canal. Nevertheless, there are several outstanding issues that warrant discussion as they relate to the potential size of earthquakes that may occur on this fault zone.

Foremost is whether the Limón and Pedro Miguel faults represent discrete seismogenic sources or whether they typically rupture in unison. At the surface, these two fault strands are not colinear zones but rather have different strikes and near-surface geometries (Fig. 2). As discussed earlier, the Limón fault is mapped as two separate strands separated by a right step (Fig. 2). The right-step along the Limón fault occurs within a topographically elevated section, whereas a right step should be a zone of extension. This observation suggests that the apparent right-step at the surface does not reflect extension across a right step at depth but may be more related to the shallow near-surface dip of the fault, as exposed in our trenches (Fig. 4). Although we have no subsurface structural information on the northern strand of the Limón fault, the surface trace is linear, suggesting a fairly steep dip. It is possible that the low easterly dip of the southern strand merges easterly with a high-angle northern strand at depth, allowing for a more linear fault at depth. Probably

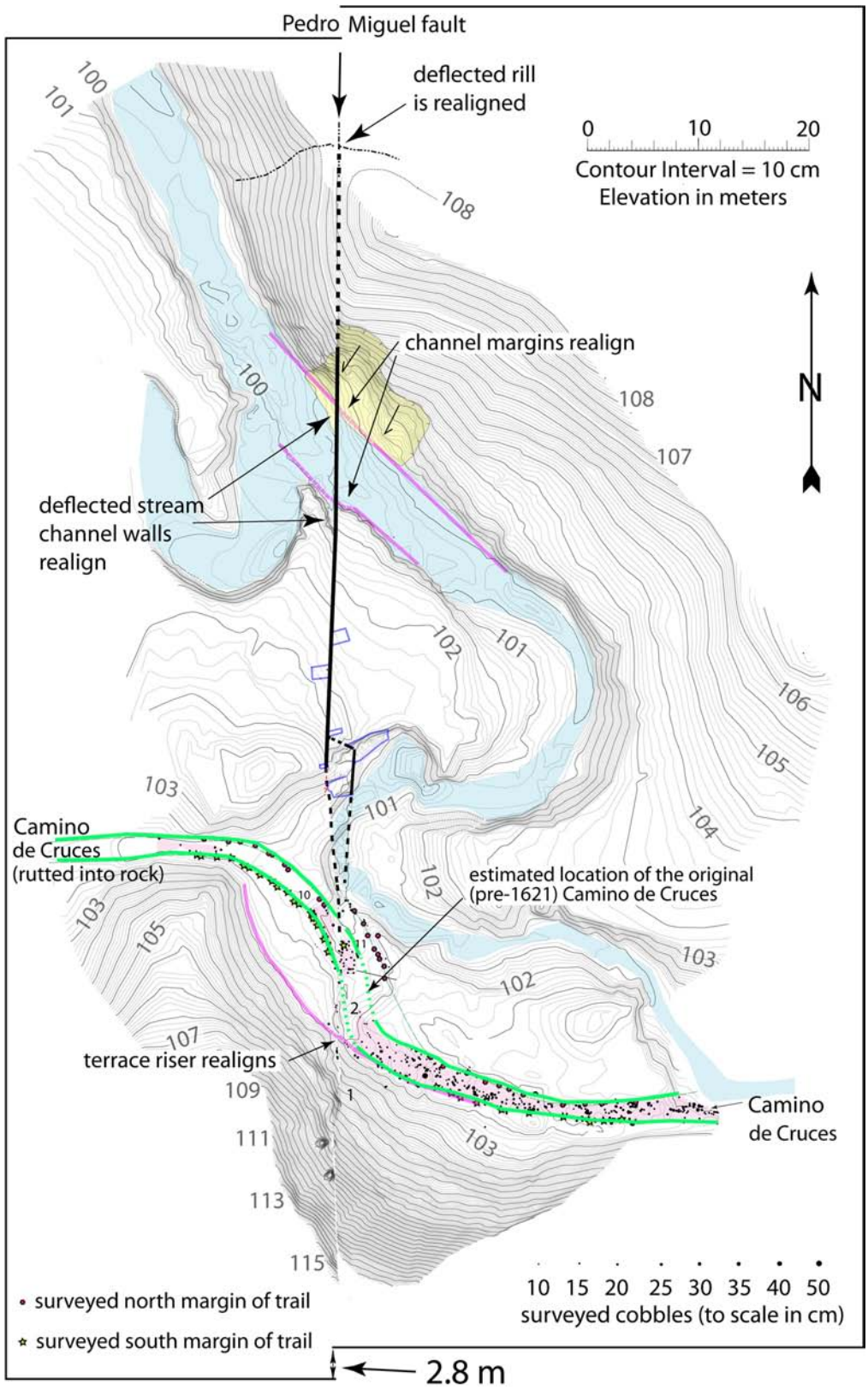

Figure 21. Reconstruction of the topographic map of Figure 19 to realign rills, channel walls, and the major stream deflection. This required 2.8 m of back-slippage. Note that the Camino de Cruces still has a deflection in its alignment, which presumably allowed for the burro trains to transition from the steep trail notch cut into rock to the west as the trail transitioned onto the edge of the low terrace east of the fault. The trail deflection is now a symmetric double bend, as opposed to a strong kink associated with the original trail cobbles. The color version of this figure is available only in the electronic edition.

only detailed microearthquake studies along the Limón fault can resolve whether this is true.

If the Limón fault does have a steeper dip at depth, with the deep, seismogenic portion of the southern trace of the fault zone more to the east than its surface trace, this could explain why the Limón and Pedro Miguel faults have probably ruptured together in some past events. The Pedro Miguel fault was nearly vertical in all exposures north of the Panama Canal. This configuration would make the overall zone considerably straighter than the surface traces of the faults would imply. We suggest that the southern part of the Limón fault has inherited its geometry from an earlier history of normal faulting. The Limón fault may have been reactivated in the Quaternary as a strike-slip fault, with its surface geometry heavily influenced by the earlier movement history and consequent fault geometry.

The slip rate of this zone is also a topic that requires some discussion. The Mid-Holocene to present rate on the Limón fault is estimated at about 6 mm/yr from offset of a terrace riser inset into a 5000-year-old terrace remnant, although this age is dependent on a single OSL date. The Late Holocene rupture history may argue for a lower rate of about 3–4 mm/yr (1.5–2-m displacements every 400–600 years), although the record of only three events is likely too short to assess a rate. In both cases, the Limón fault is a moderately fast fault in the Holocene, which is what drives the current seismic hazard associated with this structure.

For the Pedro Miguel fault, we used a speculative climate-driven incision model to date the clearly defined channel offsets and resolve a long-term rate of about 5 mm/yr. However, there are no reliable direct ages on any of the large offset features, so this rate requires further assessment.

A short-term rate can be derived from the trenching observations along the Pedro Miguel fault at Cocolí. For the T14 site, we consider two alternative interpretations. We consider the possibility that the displacement amounts were similar for all events (i.e., characteristic slip), which implies that the unit 9 gravels are offset by all three events. Alternatively, if unit 9 was offset in only the past two events, the penultimate event was larger than the MRE (event 1). Here, we discuss each scenario, along with their inferences on rate and assuming that the short-term rate adequately reflects the long-term rate.

For one model, we assume characteristic slip—that is, each of the past slip events had similar displacements at Cocolí. For the age model, we take the youngest dates from each unit and construct probability distributions for the event ages, resulting in surface ruptures around AD 455, AD 720, and the MRE poorly constrained to post-AD 900 (see Fig. 22). Using the observation of the offset Camino de Cruces, the MRE must be historical and is likely the large historical earthquake of AD 1621. From this, and assuming that we did not miss an event, it is evident that earthquake recurrence has been irregular, with interval recurrence between events of about 265 and 920 years. If representative of the long term, this suggests a return period of about 600 ± 330 years. However, because the unit 6 gravel channel clearly truncates and erodes all earlier units and because slip on unit 9 is a minimum, it is possible that another event occurred between deposition of units 7 and 6 for which we have no preserved evidence in the T14 site. If this is the case, then we are likely underestimating the rate and overestimating the return period, and the Pedro Miguel fault could be quasi-episodic in its behavior. However, because we have no observations that support such a model, we do not discuss it further.

Taking the timing of the three known events and assuming characteristic behavior of 2–3 m per slip event for the

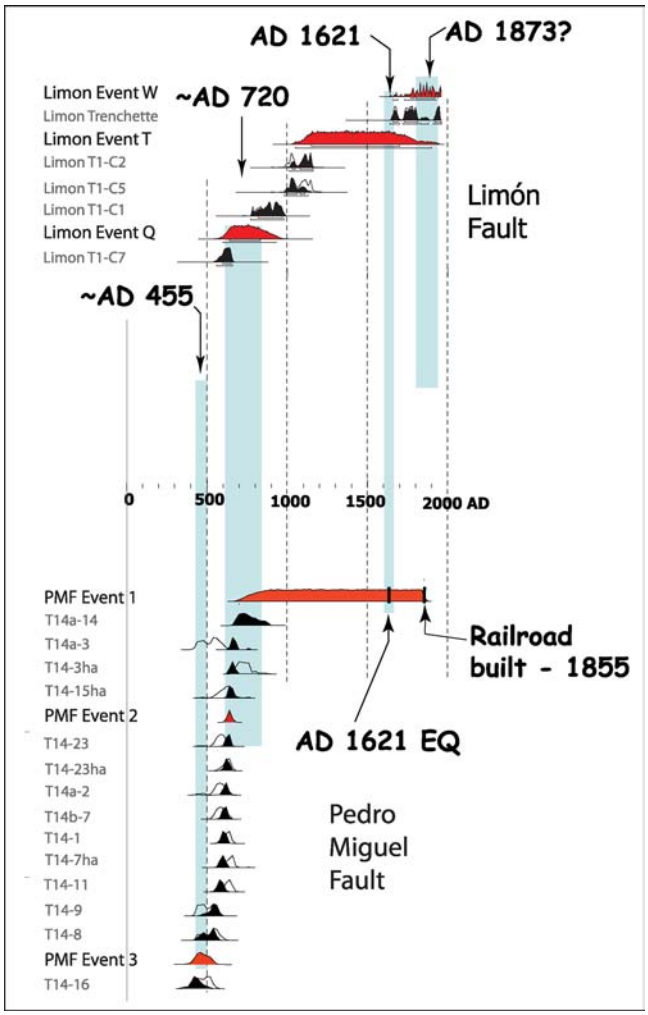

Figure 22. Comparison of dates of surface ruptures from the Limón and Pedro Miguel paleoseismic sites. Note that event Q at the Limón fault has a very similar age to event 2 on the Pedro Miguel fault, suggesting that these two faults may have ruptured together in that event. Also note that the Limón fault sustained two ruptures in the past 1 ka, whereas we only recognize event 1 for the Pedro Miguel fault. Finally, note that event 3 on the Pedro Miguel fault is older than the dated record for the Limón fault, but we speculate that it may correspond to the undated event N at the Limón site. The color version of this figure is available only in the electronic edition.

Pedro Miguel fault, we estimate an average slip rate of about 4.5 mm/yr with an uncertainty of about 50%. Considering the elapsed time since the MRE, it is unreasonable to argue for increasing the rate substantially. Nevertheless, this short-term rate is similar to that inferred from interpretation of the geomorphology and incision history.

An alternative model is to assume that the penultimate event was large and that slip on the unit 9 channel reflects just the past two events. This is based on the displacement of unit 9 along fault 2 of at least 3 m, with additional significant slip likely occurring on fault 1. Also, the MRE produced slip on only fault 1 at this site, whereas the penultimate event produced slip on both faults 1 and 2. This observation alone argues that the MRE was smaller than the penultimate event. For this scenario, we used about 5 m of slip in the penultimate event ($\geq$ 3 m on fault 2 and 2 m on fault 1, similar to the MRE). Again, using the average timing between events and a displacement value of 3–5 m suggests a slip rate of about 6.7 mm/yr (3–5 m on average every 600 years), and it could be larger if event 3 was also large. However, we believe that this provides a reasonable upper bound to the slip rate on the Pedro Miguel fault if the past 1600 years are a reasonable representation of the long-term average.

In summary for the Pedro Miguel slip rate, the Late Holocene rupture history is consistent with a slip rate in the half centimeter per year range, but, because the events have been fairly irregular in their timing and because the displacement per event may have varied between 2.5 and $>$ 5 m, there is a large uncertainty associated with these estimates. We consider the past 1600 years to be consistent with a best-estimated rate in the 4–7 mm/yr range, although, it is possible that the past 1600 years is an insufficient length of time to estimate a slip rate for this zone.

Figure 22 also plots the probability distributions for the event ages for the Limón and Pedro Miguel faults. The oldest event on the Pedro Miguel fault at approximately AD 455 is older than any of the events recorded for the Limón fault. However, the penultimate Pedro Miguel event and the third Limón fault event have very similar ages at approximately AD 700 and may represent rupture of the entire onshore zone. The MRE for the Pedro Miguel has a large uncertainty in its age when inferred strictly from the radiocarbon dating, but the offset of the Camino de Cruces shows that it is almost certainly the historical earthquake of AD 1621. Similarly, the penultimate Limón event is poorly constrained but overlaps with the penultimate Pedro Miguel event, suggesting that they could have ruptured together. In contrast, the MRE for the Limón fault is certainly younger than the 1621 earthquake and likely represents rupture of only the Limón fault in the late 1800s. Taken together, the data allow the Limón and Pedro Miguel faults to fail together but also indicate that the Limón fault may fail independently from the Pedro Miguel fault, as may have occurred in 1873 or during an aftershock of 1882.

Seismic Hazard Considerations for Central Panamá

The Panamá Canal system and Panamá City are at significant risk from a large earthquake on either the Limón–Pedro Miguel or the Río Gatún faults. The Pedro Miguel fault crosses the Panamá Canal between the Pedro Miguel and Miraflores locks and, based on extensive work onshore near the canal and in Miraflores Lake itself, no existing Canal structures appear to directly overlie the fault (Earth Consultants International, 2007; Technos, Inc., 2006). Thus, the hazard from the Pedro Miguel fault is largely one of shaking and its consequent effects. As Panamá City lies only a few kilometers from the Pedro Miguel fault, renewed activity on this fault could cause substantial damage to structures that were not designed for strong shaking.

Implications for Regional Tectonics

The ~5 mm/yr slip rate for the dextral Pedro Miguel fault, along with a similar sinistral rate for the Rio Gatún fault (Earth Consultants International, 2005), indicate that central Panamá is internally deforming at a significant rate. This observation invalidates the assumption of Trenkamp *et al.* (2002), which treated Panamá as a stable block. The basis for this inference was that the regional GPS rates observed from the Central and South America (CASA) network generally indicated rates in the multiple cm/year range, whereas the uncertainties from this campaign network were about a cm/yr. Although the GPS data did suggest some internal deformation of Panamá, the rates were generally lower than the uncertainties, so they were ignored. A first-order conclusion from our work is that the rates are sufficiently high that we believe they should be considered in local and regional tectonic modeling.

Rockwell *et al.* (2010) developed a new block model for the deformation of central Panamá, where pure shear strain resulting from the collision of Central and South America is partly accommodated by the conjugate faults in central Panamá, as well as by folding and thrusting in eastern Panamá and the northward oroclinal flexing of Panamá into the Caribbean. In their reevaluation of the CASA data, they found that western Panamá is converging with Panamá City at about 8 mm/yr, consistent with an active Pedro Miguel fault. An interesting conclusion of the block model is that the Pedro Miguel fault is largely driven by continued shortening in westernmost Panamá and not by the northward oroclinal flexing of the peninsula (Rockwell *et al.*, 2010) which results in left-lateral slip in the Darien region to the east (Coates *et al.*, 2004).

Conclusions

The Pedro Miguel and Limón faults comprise potentially hazardous seismic sources to central Panamá, with a rate of right-lateral faulting estimated at 4–7 mm/yr. Both the Pedro Miguel and Limón faults have been historically active, with multimeter offsets of small channels, rills, and

the historical Camino de Cruces. Although the fault passes through the Panamá Canal between the Pedro Miguel and Miraflores locks, missing all critical structures, its location and rate of activity is a factor in expansion of the Panamá Canal and its new lock system. The close proximity of Panamá City to this active fault zone and the lack of consideration of earthquake loads in structural design codes make this a particularly hazardous condition should the fault rerupture before the current building stock is replaced with stronger, more earthquake-resistant construction.

Data and Resources

All data used in this paper were generated by us during the seismic hazard assessment of the Panamá Canal. Additional trench logs included in the referenced Earth Consultants International, Inc. consulting reports are available from the senior author. Radiocarbon dates were generated by the Center for Accelerator Mass Spectrometry facility at Lawrence Livermore National Laboratory, and optically stimulated luminescence (OSL) results were generated from the OSL laboratory at Cincinnati University.

Acknowledgments

The work reflected in this paper was the result of many people's hard work and support over several years. We especially want to thank the Engineering Division of the Panamá Canal Authority (ACP), Luis Alfaro and Maximillian DuPuy, and the many geologists and engineers in the group who all rendered valuable assistance and advice. Many geologists from Earth Consultants International (ECI) also participated in various ways, and we thank them and ECI for their contributions. Requests for consulting reports prepared by ECI and Technos, Inc. and for the Westman translation of Salcedo (1640) should be directed to Pastora Franceschi at the ACP. We thank Hugh Cowan and James Lienkaemper for excellent reviews that led to substantial improvements in the presentation of this paper. We also benefited from the extensive field and report reviews conducted by the ACP's Geotechnical, Structural, Seismic, and Paleoseismic Advisory Boards and Peer Reviewers, but the final interpretations and conclusions in this paper are ours.

References

Bard, E., B. Hamelin, M. Arnold, L. Montaggioni, G. Cabioch, G. Faure, and F. Rougerie (1996). Deglacial sea-level record from Tahaiti corals and the timing of global meltwater discharge, *Nature* **382,** 241–244.

Bronk-Ramsey, C. (2001). Development of the radiocarbon program OxCal, *Radiocarbon* **43,** no. 2A, 355–363.

Bronk-Ramsey, C. (2005). *Radiocarbon program OxCal version 3.10*, available at https://c14.arch.ox.ac.uk/login (last accessed December 2007).

Coates, A. G., L. S. Collins, M. Aubry, and W. A. Berggren (2004). The geology of the Darien, Panamá, and the Late Miocene–Pliocene collision of the Panamá arc with northwestern South America, *Geol. Soc. Am. Bull.* **116,** 1327–1344.

Collins, L. S., A. G. Coates, W. A. Berggren, M. Aubry, and J. Zhang (1996). The Late Miocene Panamá isthmian strait, *Geology* **24,** no. 8, 687–690.

Cowan, H. (1999). Design earthquakes for the southeast area of the canal basin, Panamá, Consulting report to the Authoridad Canal de Panamá, 35 pp.

Cowan, H., R. L. Dart, and M. N. Machette (1998). Map and Database of Quaternary faults and folds of Panama and its offshore regions: A project of the International Lithosphere Program Task Group II-2, Major Active Faults of the World, *U.S. Geological Survey Open File Report 98-779*, 41 pp.

Earth Consultants International, Inc. (ECI) (2005). *Paleoseismic investigation of the Gatún and Limón faults in Central Panamá*, ECI Project No. 2505; consulting report prepared for the Autoridad del Canal de Panamá, Project No. 2505, 30 September 2005, 89 p.

Earth Consultants International (ECI) (2006). *Geomorphic evaluation of the Miraflores, Pedro Miguel, Azota, and Caballo faults, Central Panamá*, consulting report prepared for the Autoridad del Canal de Panamá, Project No. 2614.01, November 2006, 116 p.

Earth Consultants International (ECI) (2007). *Paleoseismic trenching of the Pedro Miguel fault in Cocolí, located immediately southwest of the Panamá Canal, Panamá*, consulting report prepared for the Autoridad del Canal de Panamá, Project No. 2614.02, February 2007, 66 p.

Earth Consultants International (ECI) (2008). *Quantitative characterization of the Pedro Miguel fault, determination of recency of activity on the Miraflores fault, and detailed mapping of the active faults through the proposed Borinquén Dam location*, consulting report prepared for the Autoridad del Canal de Panamá, Project No. 2708.05, 31 January 2008, 45 p.

Jones, S. M. (1950). Geology of Gatún Lake and vicinity, Panamá, *Bull. Seismol. Soc. Am.* **61,** 893–922.

Mann, P., and J. Corrigan (1990). Model for Late Neogene deformation in Panamá, *Geology* **18,** 558–562.

Mann, P., and R. A. Kolarsky (1995). East Panamá deformed belt: Structure, age, and neotectonic development, in P. Mann (Editor), Geologic and Tectonic Development of the Caribbean Plate Boundary in South Central America, *Spec. Pap. Geol. Soc. Am.* **295,** 111–130.

Peraldo, G., and W. Montero (1999). *Sismología histórica de América Central*, Publicación No. 513, Instituto Panamericano de Geografía e Historia, México, D.F., 347 p.

Petersen, M., E. Schweig, C. Mueller, S. Harmsen, and A. Frankel (2005). *Preliminary update of the probabilistic seismic hazard analysis for sites along the Panamá Canal Zone*, 25 p.

Ramsey, C. B. (2000). *OxCal Program Ver. 3.5*, Radiocarbon Accelerator Unit, University of Oxford, available at: http://units.ox.ac.uk/departments/rlaha/orau/06_01.htm (last accessed December 2007).

Reimer, P. J., M. G. L. Baillie, E. Bard, A. Bayliss, J.W. Beck, C. Bertrand, P. G. Blackwell, C. E. Buck, G. Burr, K. B. Cutler, P. E. Damon, R. L. Edwards, R. G. Fairbanks, M. Friedrich, T. P. Guilderson, K. A. Hughen, B. Kromer, F. G. McCormac, S. Manning, C. Bronk, R. W. Reimer, S. Remmele, J. R. Southon, M. Stuiver, S. Talamo, F. W. Taylor, J. van der Plicht, and C. E. Weyhenmeyer (2004), IntCal04 terrestrial radiocarbon age calibration, 0-26 cal kyr BP, *Radiocarbon* **46,** 1029–1058.

Rockwell, T., R. Bennett, E. Gath, and P. Francesci (2010). Unhinging an indenter: A new tectonic model for the internal deformation of Panama, *Tectonics* 29**,** TC4027, doi 10.1029/2009TC002571.

Salcedo, Requejo J. (1640). Relación histórica y geográfica de la Provincia de Panamá, in *Relaciones Históricas y Geográficas de America Central*, Tomo VIII, Librería General de Victoriano Suarez, Madrid, 1908, 311 p. (*Historical and geographical report of the Province of Panama*: 1947 translation by Alice E. Westman, available from the Panama Canal Authority [ACP].)

Schweig, E., H. Cowan, J. Gomberg, T. Pratt, and A. TenBrink (1999). Design earthquakes for the evaluation of seismic hazard at Gatún Dam and vicinity, Report to the Panamá Canal Commission for Interagency Agreement Number CNP-93786-NN-29 between the Panamá Canal and the U.S. Geological Survey (9 August 1999), 60 p.

Silver, E. A., D. L. Reed, J. E. Tagudin, and D. J. Heil (1990). Implications of the north and south Panamá thrust belts for the origin of the Panamá orocline, *Tectonics* **9,** no. 2, 261–281.

Stewart, R. H., J. L. Stewart, and W. P. Woodring (1980). Geologic map of the Panamá Canal and vicinity, Republic of Panamá, *U.S. Geol. Surv. Misc. Invest. Series, Map I-1232*, scale: 1:100,000.

Technos Inc. (2006). *Final Report Geophysical Investigations for the Third Set of Locks Project, Panama Canal, Panama*, consulting report prepared for the Panama Canal Authority, Project No. 06-150, 22 September 2006, 120 p.

Trenkamp, R., J. N. Kellogg, J. T. Freymueller, and H. P. Mora (2002). Wide plate margin deformation, southern Central America and northwestern South America, CASA GPS observations, *J. S. Am. Earth Sci.* **15,** 157–171.

Woodring, W. P. (1957). Geology and paleontology of Canal Zone and adjoining parts of Panama, *U.S. Geol. Surv, Profess. Paper 306-A*, 145 p.

Earth Consultants International, Inc.
1642 East 4th Street
Santa Ana, California 92701
(T.R., E.G., T.G., C.M., D.V., C.L., T.D., A.C., E.W.)

Department of Geology
University of Cincinnati
Cincinnati, Ohio 45221
(L.A.O., M.F.)

Geological Sciences
San Diego State University
San Diego, California 92182
(P.W.)

Autoridad del Canal de Panamá
Balboa, Republic of Panamá
(P.F.)

Manuscript received 27 October 2009